4-2019

Fiber-Reinforced Polymer Bridge Girders for Extremely Aggressive Environments

Abdellah Emad Azeez

FIBER-REINFORCED POLYMER BRIDGE GIRDERS FOR EXTREMELY AGGRESSIVE ENVIRONMENTS

By

Abdellah Emad Azeez

A Thesis Submitted to the College of Engineering, Department of Civil Engineering

In Partial Fulfillment of the Requirements for the Degree of

Master of Science in Civil Engineering

Embry-Riddle Aeronautical University

Daytona Beach, Florida

April 2019

FIBER-REINFORCED POLYMER BRIDGE GIRDERS FOR EXTERMELY AGGRESSIVE ENVIRONMENT

By

Abdellah Emad Azeez

This thesis was prepared under the direction of the candidate's Thesis Committee Chair, Dr. Jeff Brown, Associate Professor of Civil Engineering, Daytona Beach Campus, and Thesis Committee Members Dr. Ashok Gurjar, Professor of Civil Engineering, Daytona Beach Campus, and Dr. Dan Su, Assistant Professor of Civil Engineering, Daytona Beach Campus, and has been approved by the Thesis Committee. It was submitted to the Department of Civil Engineering in partial fulfillment of the requirements for the degree of Master of Science in Civil Engineering

Thesis Review Committee:

Jeff Brown, Ph.D.
Committee Chair

Ashok H. Gurjar, Ph.D.
Committee Member

Dan Su, Ph.D.
Committee Member

Ashok H. Gurjar, Ph.D.
Graduate Program Coordinator

Ashok H. Gurjar, Ph.D.
Department Chair

Maj Mirmirani, Ph.D.
Dean, College of Engineering

Christopher D. Grant, Ph.D.
Vice Provost of Academics Support

4/24/19

Date

Acknowledgements

First I would like to thank my research advisor Dr. Jeff Brown, Associate Professor of Civil Engineering at Embry-Riddle Aeronautical University. Dr. Brown is the kind of professor who never turns-down students when they ask for help or guidance. His office is always open to anyone in need of advice. This thesis would not be accomplished without his knowledge and support.

I would also like to acknowledge the committee members, Dr. Ashok Gurjar, Professor of Civil Engineering, Chair of the Department of Civil Engineering, and Program Coordinator for the B.S. in Civil Engineering and Dr. Dan Su, Assistant Professor of Civil Engineering Department. I am very thankful for their valuable observations and comments on this thesis.

I would also like to thank the Department of Civil Engineering for providing me with the resources and giving me the chance to take part in this study research. I would also like to acknowledge a staff member of Embry-Riddle Aeronautical University, Rosa A. Criado, Administrative Assistant, Department of Civil Engineering, for all her help over my college years.

Finally, I must show my very deep gratefulness to my family and to my friends for being my support during my college journey. Without them, I would not have reached my goal towards graduation. Thank You.

Abstract

In 2012, the federal government estimated that $17.5 billion was spent on inspection, rehabilitation, maintenance, and replacement of the nation's bridges. While the average lifespan of steel and reinforced concrete bridges is 50 years, certain bridges subjected to extremely aggressive marine environments may not reach this desired target. This research paper investigates using fiber-reinforced polymer (FRP) materials as primary bridge girders in medium span bridges (30 ft. to 75 ft.). The goal of this research is to identify the most efficient and cost-effective alternative for these corrosion-resistant materials and potentially extend the lifespan of these bridges up to 75 years. Three distinct profiles were investigated in this research: U-shaped, concrete-filled FRP tubes, and Double Web I-Beams (DWB). Finite Element Modeling (FEM) was used to study the overall stiffness of FRP girder bridges with a cast-in-place concrete deck. Girder distribution factors for moment were also computed using reliability analysis tools and FEM. These results were then compared to existing AASHTO methods. Once the most efficient cross-section was identified (U-shaped girder), a preliminary study investigating the vacuum infusion manufacturing process was conducted to verify that the required thicknesses of FRP can be achieved. Simple bending tests were completed on small-scale FRP beams to demonstrate the strength capacity and evaluate any difficulties using the vacuum infusion process (VIP). The results in this research study conclude that the U-shaped bridge girder is the most cost-effective alternative, yet fabrication remains challenging and complicated.

Table of Contents

Figures

Tables

Chapter 1 Introduction

This research paper investigates the use of fiber-reinforced polymer (FRP) in medium-span bridge girders subjected to extremely aggressive environments. In the state of Florida, extremely aggressive environments for bridges typically refers to salt water environments. Medium-span bridges (30 ft – 75 ft span lengths) with low clearance to the bridge girders are especially susceptible to corrosion damage. Bridges in the United States are designed to have a lifespan of only 50 years. New AASHTO requirements recommend a service-life of 75 years. Keeping these bridges safe and reliable requires frequent inspection and maintenance. Using FRP materials in place of traditional reinforced concrete or steel for the bridge girders should help extend the useful life of bridges to a desired service-life of 75 years.

1.1 Background

Bridges come in all different shapes and sizes. They all serve the same purpose. Bridge construction started during the Roman Empire. Since then, bridges have developed to become an essential part of society's infrastructure. Some bridges are iconic, and they represent a part of a

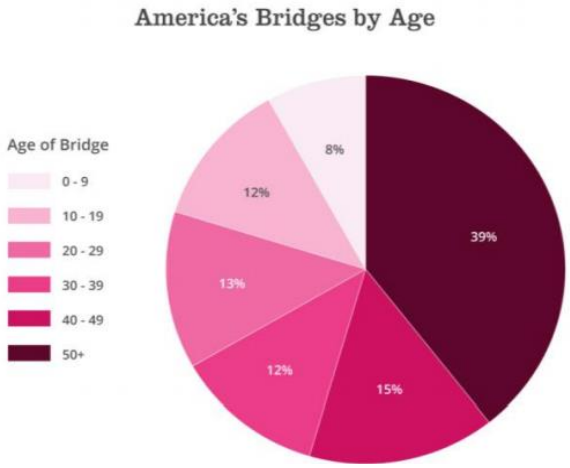

Figure 1-1 Percentage of the age groups of the bridges in the United States as of 2017 (*ASCE, 2017*).

country's culture. The American Society of Civil Engineering (ASCE) has reported that there are 614,387 bridges in the United States as of 2017.

As shown in Figure1, almost 40% of these bridges are 50 years or older. In 2016, 9.1% of the bridge are reported as structurally deficient. Bridges are designed to have a lifespan of 50 years. The ASCE has reported that the average bridge in the United States is 43 years old (ASCE, 2017). Statistical analysis shows that about 90% of bridges in the United States have maximum spans of 100 ft (30.5 m) while 67% of bridges have spans in the 20 ft-to-60 ft (6.1-to-18.3 m) range (Hurd, 1985).

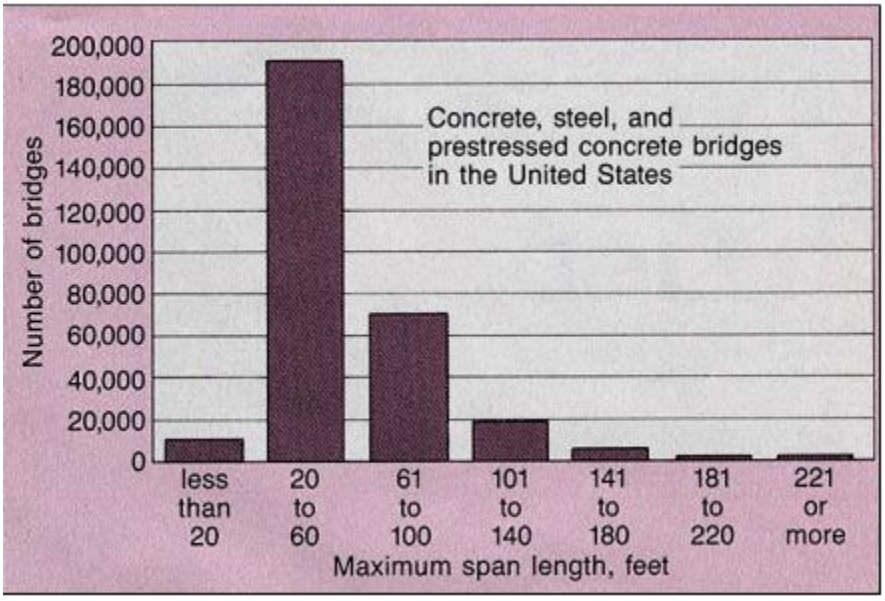

Figure 1-2 Number of bridges in the United States based on their span length (*Hurd, 1985*).

In 2006, $11.5 billion was spent on inspection, rehabilitation, maintenance, and replacement of the nation's bridges. In 2012, the federal government estimated that $17.5 billion was spent on bridges. Even though there was an increase in the spending, funds in the country's bridges are still deficient. Based on the most recent federal estimate, $123 billion is needed for rehabilitation projects for the nation's bridges (ASCE, 2017).

1.2 Statement of the Problem

Steel and reinforced concrete are affected by several environmental deterioration factors. These factors can reduce the safety and reliability of a bridge. Causes of reinforced concrete bridge deterioration include:

- Chloride contamination by de-icing salts, saline air and seawater;
- Sulphate attack;
- Thermal effects (freeze/thaw action);
- Poor quality concrete;
- Insufficient concrete cover;
- Lack of maintenance;
- Alkali-silica reactions;
- Ineffective drainage;

The Strategic Highway Research Program has stated that Alkali-silica reaction (ASR) is the main cause of concrete cracking and deterioration in the United States. When silica and alkali combine, they produce a gel reaction product. This gel reaction expands in a moist environment, and that results in cracks in concrete. In dry regions, like the southwest of the United States, the gel reaction product from ASR tends to shrink. This shrinkage also causes the concrete to crack. Other factors that control the rates of deterioration of the reinforced concrete are reinforcing bar corrosion, carbonation, and freeze-thaw cycle (AISI, 2016). This study focuses more on the environmental factors and the possible solutions rather than the mechanism chloride intrusion.

Corrosion is one of the biggest issues facing reinforced concrete and steel bridges. The corrosion can be classified into three levels of severity in the environment, mild, moderate, and

severe. Sometimes, it is difficult to distinguish between the moderate and severe environment because salt can be carried several miles away from the shorelines by winds and storms.

1.3 Background and Justification

The American Society of Testing and Materials (ASTM) has conducted a study to determine the corrosion rate of carbon steel and zinc in different regions of North America. The figure below shows the loss of material per two-years of exposure.

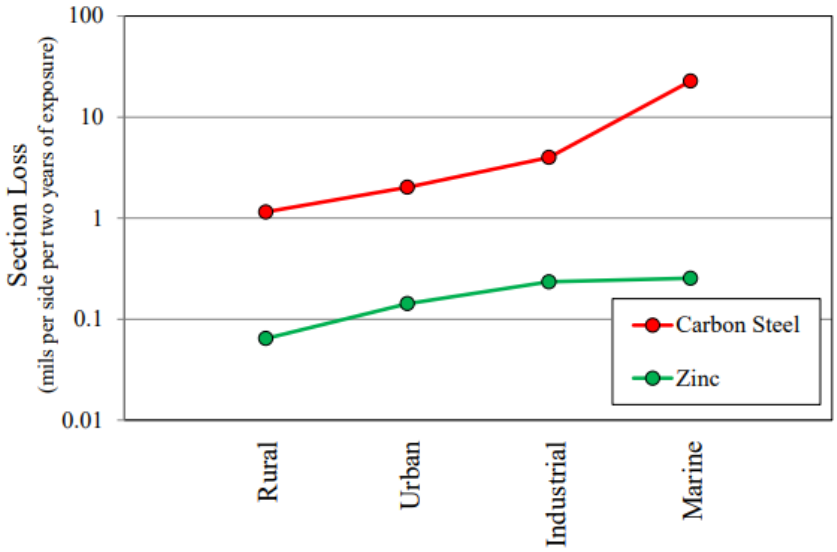

Figure 1-3 Loss of carbon steel and zinc in four different environments. Where the loss was measured mils/side/2years (*Hartmann, 2015*).

4-in (101.4 mm) by 6-in (152.4 mm) panels were used in the study. The panels were exposed two years each, and the mass loss was expressed in mils per two-year, per side. The samples were not directly in contact with the deicing salts. If the bare steel and zinc were in contact with the salt that would represent the corrosion rate for the marine environment even in non-marine sites (Hartmann, 2015).

When the time comes for inspection, corrosion is not easy to predict in the reinforcing bars that are behind the concrete cover. The Tutti model can be used to estimate the residual service life of corroding structures (Figure 4). Tutti's Model is divided into two stages: Initiation and Propagation. Initiation is the stage where externally harmful substance enters into the concrete cover. Propagation period is where the substance penetrates into the concrete cover to depassivate the steel. The time for the corrosion initiation period can be determined using laws of diffusion of chlorides and carbon dioxide; however, the propagation portion can be determined theoretically rather than quantitatively. The reason behind this concern is that there is not enough literature on deterioration rates (ASTM, 1990).

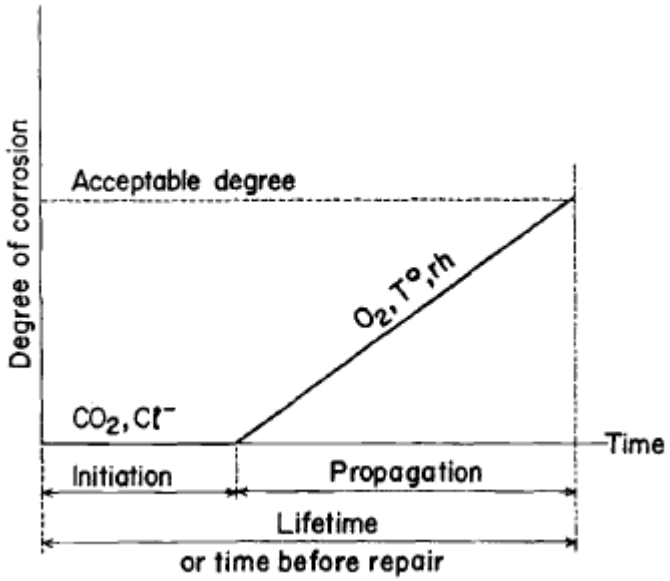

Figure 1-4 Tutti's Model used to predict the residual service life of deteriorated RC structures (ASTM, 1990).

A nationwide survey shows that there are 14 states that use precast, nonprestressed, concrete channel beams. Arkansas State Highway and Transportation Department (AHTD) stated in their inventory that there are 389 in-service brides using precast channel beams that were constructed using the 1952 AHTD bridge details. During the nationwide investigation, 2,000 beams in 95% of these concrete channel-beam bridges were inspected. The results shows that 60.4% of the

beams experience longitudinal cracking at the reinforcing steel level. The main cause of these cracks is corrosion.

1.4 Purpose of the Study

The purpose of this research is to investigate three alternative FRP cross-sections: -U-shaped, concrete-filled FRP tubes, and Double Web Beams (DWBs) with emphasize on the DWB section. A conceptual design study was completed for medium-span bridge girders with lengths ranging between 30 ft (9.1 m) and 75 ft (22.9 m). The goal of the first phase of this study was to select an alternative that is the most efficient and cost-effective among the three existing FRP cross-sections.

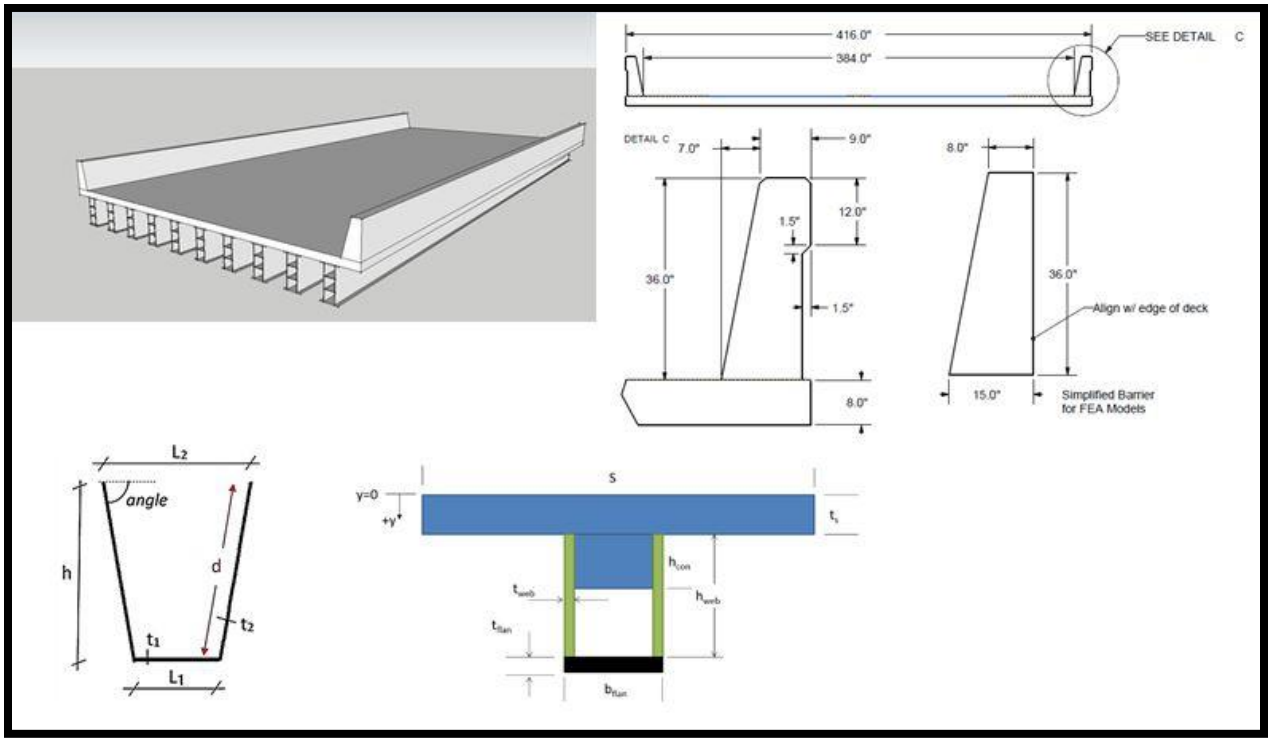

Figure 1-5 DWB and U-Shaped bridge girder cross-sections

In this study, the distribution factor for FRP was calculated using tools from reliability analysis and existing research studies. Ultimately, the results for the distribution factor were compared to the AASHTO LRFD-7 and LRFD-FRP. The goal was to calculate the distribution factor of the U-shaped and DWB cross sections using a Finite Element Model (FEM) and the reliability analysis method.

The last part of this study was to manufacture small-scale FRP panels to demonstrate the vacuum infusion process (VIP) and assess the overall suitability of the method for FRP panels up to 1-inch thick. Small beam samples were obtained from these panels and simple bending tests were performed to validate the strength properties of the FRP.

Chapter 2 Review of the Relevant Literature

A composite material is a combination of at least two different constituent materials that have different thermomechanical properties. In the final product of the composite, the constituent materials remain distinct. Fiber reinforced polymer (FRP) is a special type of composite. In the FRP, the constituent materials are the reinforcement, which is generally a fibrous material, and the matrix, which is a resin in form of a polymer that bonds the fibrous particulates together.

The use of composite materials was discovered thousands of years ago in Mesopotamia (present-day Iraq). They used mud and straw in bricks and asphalt-bonded copper sheets. Some common organic resins that were used in practice are fossilized resins, tree and plants secretions, bituminous materials, and fish. Many forms of composite were used in decorations in India. In 1941, Henry Ford introduced the first soybean car. Ford developed quarter-inch-thick panels reinforced with tubular steel. Other examples of composites applications are found in common household items such as; washing machines, refrigerators, drains, etc. Throughout the twentieth century, the applications of FRP expanded to reach the aviation and naval fields (Zoghi, 2014).

2.1 Aviation Sector

Examples of composites materials in the aviation sector are fighter aircraft, helicopters, launch vehicles, small and big civil transport aircraft, satellites, and missiles. The composite materials must meet specific requirements for aerospace structures. The material must go through an extensive testing process to insure high reliability before use. Composite materials have features that make them the best candidate to be used in the aircraft industry. These unique features are: -

- Light weight due to high specific strength and stiffness.

- Fatigue resistance and corrosion resistance
- High degree of optimization through tailoring the directional strength and stiffness.
- Ability to mold large complex shapes in small cycle time reducing part count and assembly time: Good for thin-walled or generously curved construction.
- Ability to maintain dimensional and alignment stability in space environment.
- Low dielectric loss in radar transparency.
- Low radar cross-section.

Just like other materials, composites have weaknesses. The weaknesses include: -

- Laminated structure with weak interfaces: poor resistance to out-of-plane tensile loads.
- Susceptibility to impact damage and strong possibility of internal damage going unnoticed.
- Moisture absorption and consequent degradation of high temperature performance.
- Multiplicity of possible manufacturing defects and variability in material properties (Nayak, 2014).

As one of the biggest commercial airplane manufacturers, Boeing has developed a new philosophy regarding life-cycle-cost analysis. Boeing has reconsidered their design approach to include the maintenance cost and airplane availability to the life-cycle cost design. Traditionally, the life-cycle cost includes only drag, weight, noise, schedule reliability, development cost, and build cost. The new Boeing 787 program has successfully reduced the maintenance cost and increased the airplane availability. The new Boeing 787 uses composites extensively in its airframe and primary structure.

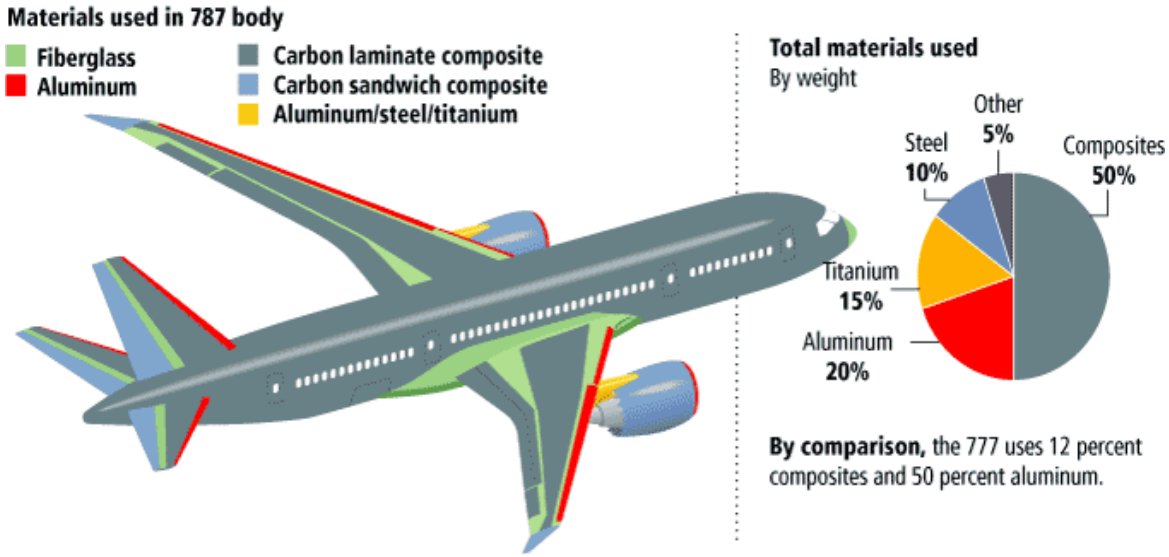

Figure 2-1 Percentage of the material that is used in Boeing 787 (*Nayak, 2014*).

As shown in the figure above, 50% of the airframe is built using composite material. Most of the composite material is carbon fiber with an epoxy matrix. The use of composite materials reduces the weight of the airplane by 20% compared to more conventional aluminum designs. The use of composite in the fuselage areas, where tension loads are high, reduces maintenance

requirements due to fatigue. The Boeing 777 requires 35% less in scheduled maintenance labor compared to non-composite structures (Nayak, 2014).

2.2 Marine Sector

Composites are also commonly used in the marine sector for building boats, race boats, superyachts, vessels for deep water, and commercial and naval craft. Composites materials offer many benefits such as: -

- Ease of use with a broad processing window
- Ideal for thick monolithic and lightweight sandwich structures
- Provides an excellent surface finish
- Offers a combination of good mechanical performance and toughness
- Supplied across a wide range of fabric and fibers

  (Cytec Industries, 2014)

The University of Hawaii has designed, analyzed, manufactured, and tested thermoplastic composite pressure vessels for securing units in the vessel against the deep-water high pressure. In their stress analysis, they generated a ply-by-ply analytical solution for thick-wall composite cylinders under external hydrostatic pressures. Then they used finite element models to verify their results. After analyzing their design, the vessels have been manufactured using APC-2/As4 thermoplastic composite unidirectional prepreg tape. The vessels were designed to withstand a hydrostatic pressure of 3.5 ksi (24.1 MPa) (Yousefpour, 2004).

Figure 2-2 Thermoplastic composite pressure vessel design and manufactured by University of Hawaii (*Yousefpour, 2004*).

2.3 Civil Engineering

The use of FRP has also extended to civil engineering structures, especially in bridge construction. The material properties of FRP make it a unique material that can be used in civil engineering structures. These properties are:

- High strength-to-weight ratio
- High stiffness-to-weight ratio
- Corrosion resistance

Reasons why FRP is not good for civil infrastructure include:

- High material cost
- Short history of applications
- Lack in the developments of established standards

The following sections provide examples of FRP bridges that were constructed between 1996 and 2007. These bridges serve as useful benchmarks for the current study and also serve to demonstrate the short-term durability and performance of the material in bridge applications.

2.3.1 No-Name Creek Bridge, Kansas

The Kansas Department of Transportation (KDOT) with the help of Kansas State University (KSU) and Kansas Structural Composites (KSCI) were able to construct the first FRP composite panel bridge, No-Name Creek Bridge. The bridge was built in 1996 and is still in service. The simple span bridge is 23 ft (7.0 m) long and consists of three panels. Each panel is a 22.5 in (572 mm) thick sandwich structure. The bridge has been subject to regular static and dynamic load tests over the years. No significant change in bridge stiffness was noted after eight years of service (Creese, 2004).

2.3.2 Sugar Grove over Dickey Creek, Virginia Route 601 Bridge

Another example of an FRP bridge structure is Sugar Grove over Dickey Creek, Route 601 Bridge, Virginia. The bridge was built in 2001. The bridge is the first to use the 36-in (914 mm) hybrid DWB beams in a bridge superstructure. It consists of eight DWB girders supporting glue-laminated timber deck panels. The bridge is 39 ft (11.9 m) long with a transverse width of

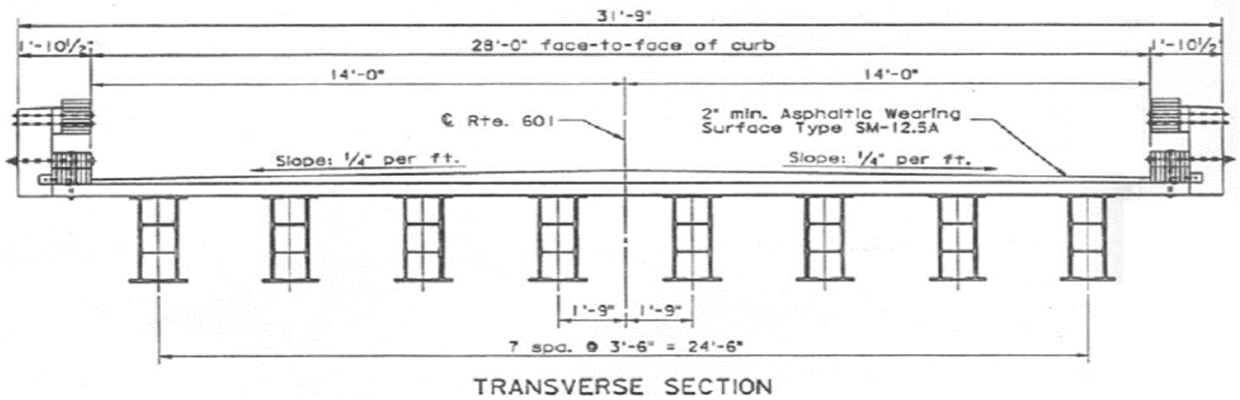

Figure 2-3 Transverse section of Route 601 Bridge, Virginia (*Cousins, 2005*)

31.75 ft (9.7 m). An asphalt wearing surface was placed on the deck. No composite action between the girders and the deck was taken into consideration when designing the bridge.

The girders were tested in the laboratory as well as in the field. Strain and deflection tests were performed to evaluate the serviceability of the bridge. The field result for the maximum deflection of the bridge was L/1110, which was lower than the AASHTO L/800 limit. The testing results showed that strength of the girder was controlled by compression failure in the flange and not shear failure (Cousins, 2005).

2.3.3 Tom's Creek Bridge, Blacksburg, Virginia

Tom's Creek Bridge is an example of a short-span bridge utilizing FRP beams as the main load carrying members. The bridge was built in 2003 with the help from Virginia Tech, Strongwell, the Virginia Department of Transportation, and the Town of Blacksburg. Twenty-four pultruded FRP girders were utilized in the construction of the bridge. The girders are 20 ft (6.1 m) in length, and they support a glue-laminated timber deck.

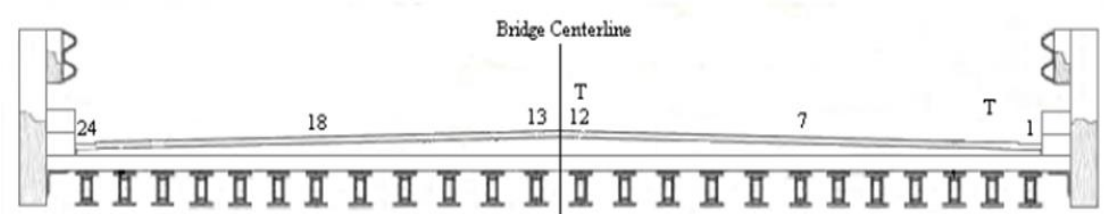

Figure 2-4 Transverse section of Tom's Creek Bridge, Virginia (*Neely, 2003*).

It was suggested to use a deflection criteria of L/425 (LRFD Specification) or L/500 (Standard Specification) because this value is consistent with AASHTO deflection control

criteria for an all-timber bridge. The Tom's Creek Bridge project helped to revise current AASHTO bridge design standards for use with FRP composite materials (Neely, 2003).

2.3.4 FM 3284, San Patricio County, Texas

The FM 2184 bridge was constructed in 2004 in Texas. The bridge was the first to use FRP U-girders to support a cast-in-place concrete deck. The bridge consisted of two 30-ft (9.1-m) simple spans and width of 32 ft (9.8 m). The manufacturing method used to construct the 24 beams was a hand lay-up method. A total of 12 girders spaced at 2.67 ft (0.8 m) on center were used for each span (Reitmann, 2007).

Figure 2-5 Hand lay-up method for San Patricio Bridge (*Reitmann, 2007*)

An experimental investigation was done on San Patricio Bridge specimens. The FRP beams consist of 37 layers of E-glass fiber oriented 0°/90° and vinylester matrix resin. The cross-section of the beams was a U-shaped with an open top and uniform thickness of 1.75 inches (44 mm).

The width of the beam is wider at mid-span than at the supports. Styrofoam was used to fill the beams from the bottom up to 9 inches (229 mm) away from the top flange (Chen, 2009).

2.3.5 FM 1684, Refugio County, Texas

In 2007, the second FRP U-shaped girder bridge was constructed in Texas. The bridge had a single span of 50 ft (15.2 m) and width of 32 ft (9.8 m). The bridge consisted of eight girders spaced at 4 ft (1.2 m) center-to-center. The total weight of each beam was roughly 5,000 lbf (Williams, 2008).

Figure 2-6 FM 1684 Bridge, Texas (*Williams, 2008*)

The VARTM method was used to manufacture the Refugio Bridge girders. 1,700 lbf of vinylester resin was used for each beam to bind 3,300 lbf of E-glass fiber as it was indicated by the manufacturer (MFG Corporation).

2.3.6 King's Stormwater Channel (KSC) Bridge

The King's Stormwater Channel Bridge is a demonstration project that was done by researchers at UC-San Diego using concrete-filled FRP tubes (CFFT). The bridge consisted of

two 33 ft (10.1-m) spans with a multi-column intermediate pier. The total length was 66 ft (20.1 m) with width of 42.5 ft (13 m)

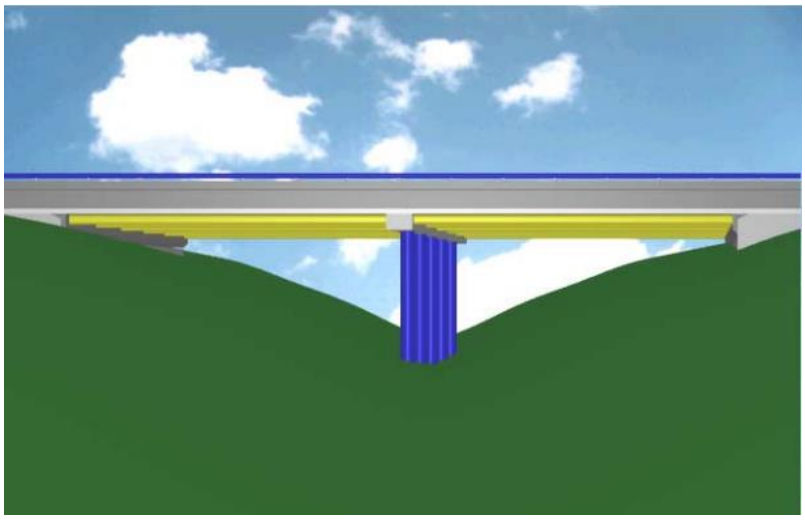

Figure 2-7 Conceptual rendering of the side view of Kings Stormwater Channel Bridge (*Zhao, 2000*)

Filament wound carbon/epoxy was used to build the longitudinal girders shells that are filled with lightweight concrete. The bridge deck used E-Glass Fiber Reinforced Polymer (GFRP) composed of pultruded trapezoidal sections. The King's Stormwater Channel Bridge was a concept for I-5/Gilman advanced composite cable stayed bridge that was never built in La Jolla, California. The King's Stormwater Channel Bridge experienced heavy traffic that caused the FRP deck to have problems. Ultimately, the bridge was replaced after 12 years of service due to

deck maintenance. California DOT reported that the CFFT girders showed no sign of any damage during the service period (Zhao, 2000).

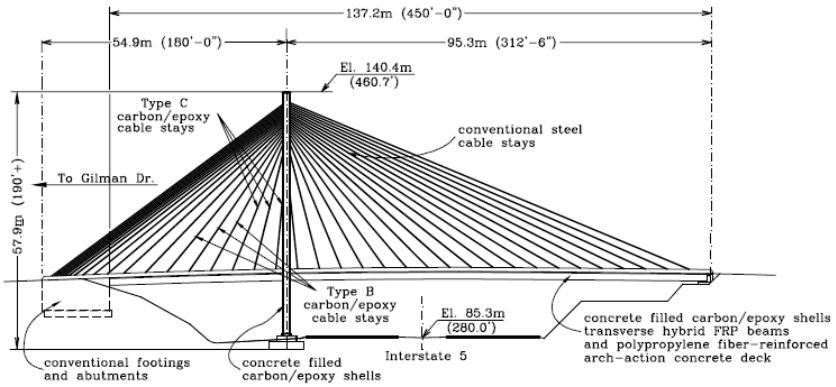

Figure 2-8 I-5/Gilman Advanced Technology Bridge (*Zhao, 2000*)

Chapter 3 Girder Alternative Analysis

This chapter describes the design requirements, limit states and design approach used to evaluate the three existing FRP cross-sections. Limitations are also addressed as part of this chapter. The FEA method was used to analyze the Girder distribution for the U-girders and the DWB sections. The results from FEA were compared to results from the AASHTO-LRFD method. The overall objective of this chapter is to locate the most efficient FRP girder available to replace typical steel and reinforced-concrete girders in medium-span bridges subjected to extremely aggressive environment.

3.1 Design Requirements

3.1.1 LRFD Loading

Table 1 shows different load types from LRFD-7 Section 3.3.2 for bridge design. These load-types were addressed in this study. Table 2 shows the unit weights for common bridge construction materials. A future wearing surface of 15 psf (0.72 kPa) was assumed to accommodate with the FDOT Structural Design Guidelines.

Table 3-1 Types of Load

Load Description	Abbreviation
Permanent Loads	
Dead load of structural components and non-structural attachments	DC
Dead load of wearing surfaces and utilities	DW
Transient Loads	
Vehicular live load	LL
Vehicular dynamic live load	IM

Table 3-2 Materials Unit Weight

Material	**Unit Weight (kip/ft^3)**
Asphalt/bituminous wearing surfaces	0.140
Lightweight concrete	0.110
Normal weight concrete	0.145
High strength concrete	$0.140 + .001\ f'_c$ *

*f'_c is the design compressive strength of concrete

The AASHTO HL-93 design live load consists of three sources: design truck, design tandem, and design lane load. In order to produce maximum weight on the bridge, the location of the truck needs be varied in the longitudinal direction. The rear axle spacing must also vary between 14 ft (4.3 m) and 30 ft (9.1 m). The design lane load is (0.64 kips/ft), and it is uniformly distributed in the longitudinal direction of the bridge. The lane load is designed to act over a 10 ft (3 m) transverse width.

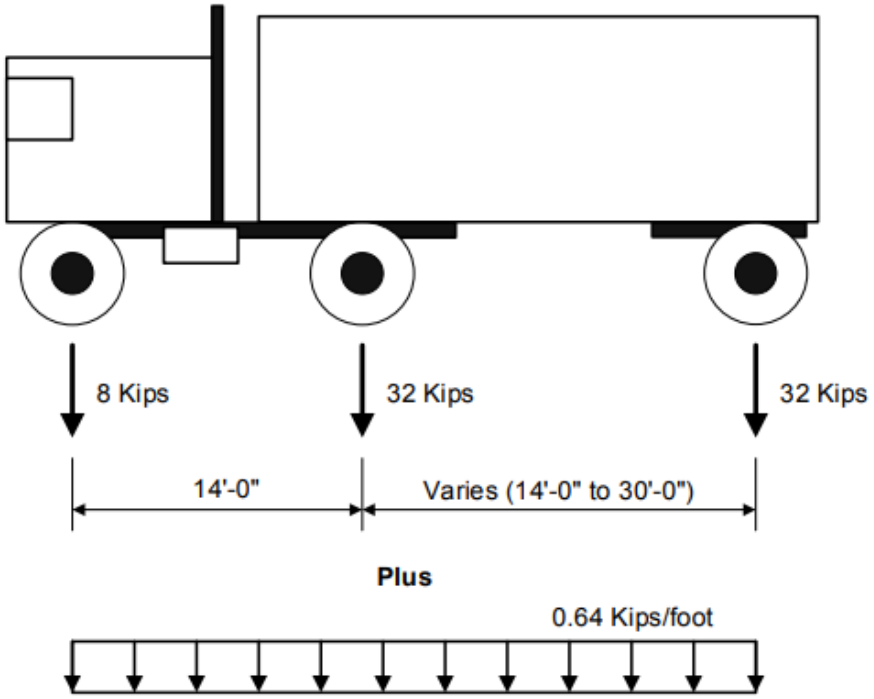

Figure 3-1 HL-93 design truck plus the design lane load as uninformed distributed load (AASHTO , 2014).

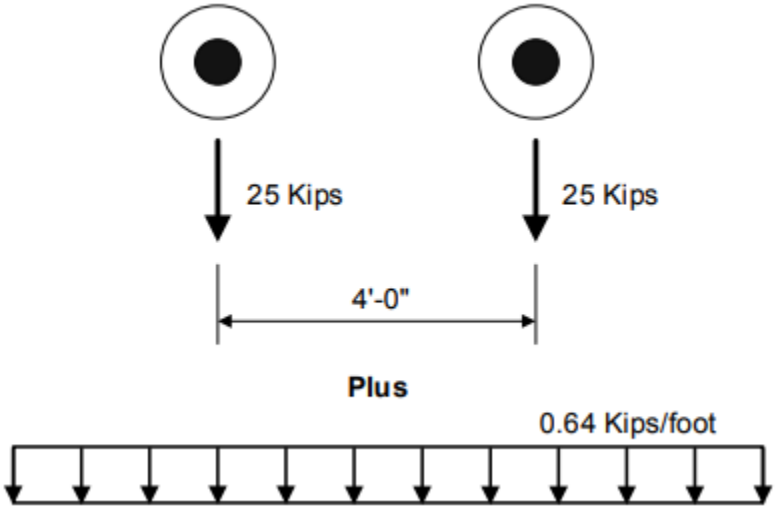

Figure 3-2 Design tandem plus the design lane load as uninformed distributed load (AASHTO,2014).

In order to account for the likelihood that the bridge will experience simultaneous loading of multiple lanes, multiple presence factors are used based on the number of loaded lanes as shown in Table 1. The multiple presence factors are not applied in the case of fatigue loading or when the approximate load distribution factors specified in LRFD-7 Sections 4.6.2.2 and 4.6.2.3 are used to obtain the maximum moments and shears for single girders. The design traffic lane is 12 (3.7 m) wide. In order to find the maximum effect due to live load, different combinations of simultaneous loading in multiple lanes is required. "The designer is required to investigate all possible combinations of simultaneous loading in multiple lanes of the bridge in order to produce the maximum effects due to vehicle live load (Brown, 2018)"

Table 3-3 Multiple presence factors associated with the number of loaded lanes

Number of Loaded Lanes	**Multiple Presence Factor**
1	1.2
2	1.0
3	0.85
>3	0.65

When evaluating the bridge to meet the deflection criteria specified in LRFD-7 Section 2.5.2.6.2, the deflection should be calculated using the larger of the following:

- That resulting from the design truck alone
- That resulting from 25% of the design truck taken together with the design lane load

For fatigue loading, the force effects are calculated using one design truck with a constant rear axle spacing of 30 ft (9.1 m).

Section 3.6.2 of LRFD-7 also establishes provisions for a dynamic load allowance (IM) that is applied to the effects generated by a static analysis of the vehicular live loading. The dynamic load allowance is computed as (1 + IM/100), where IM is obtained from the following table:

Component	IM
Deck joints	75%
All other components: • Fatigue and Fracture Limit State • All other limit states	 15% 33%

Table 3-4 Factors associated with each limit state

Limit State	Impact	LL – Tr/Tan	LL – Lane	DL	DL-FWS
LS-1: Concrete comp. stress	1.33	1	1	1	1
LS-2: Displacements	1.33	1	0	0	0
LS-3: Fatigue and creep rupt.	1.33	0.75	0	1	1
LS-4: Strength	1.33	1.75	1.75	1.25	1.5

3.1.2 Limit States Criteria

As defined by AASHTO, “a limit state is a condition beyond which the bridge or component ceases to satisfy the provisions for which it was designed”. Load and Resistance Factor Design (LRFD) limit states are classified into four main groups – service, fatigue and fracture, strength, and extreme event. Other load combinations are used to analyze a structure for certain responses, such as deflections, permanent deformations, ultimate capacity, and inelastic responses without failure (AASHTO-LRFD, 2014).

3.1.2.1 Concrete Compressive Stress

Under the Service I loading condition, LRFD-FRP Section 2.9.8 states that the concrete compressive stresses in FRP tubes shall be limited to 0.45 f'c. The reasoning behind this reduction factor is to minimize long-term deflections due to creep in the concrete.

3.1.2.2 Deflection Control

LRFD-7 Section 2.5.2.6.2 provides standard specifications for limiting deflections under service live load. For reinforced concrete, pre-stressed concrete, and steel bridges, the deflection limits are as follows:

Bridges under vehicular loads: L/800

Bridges with vehicular and pedestrian loads: L/1000

The limitation for deflection in the current study was chosen to be L/1000 because this corresponds to the most conservative deflection criteria. Deflection is the controlling limit state for most FRP bridges according to previous research. The reason behind the excessive deflection is that the FRP has a low modulus of elasticity compared to steel.

3.1.2.3 Fatigue and Creep Rupture

This limit state was derived from LRFD-FRP Section 2.7.2. The following limits should not be exceeded for the maximum longitudinal tensile stress in the FRP in order to avoid failure caused by the long-term creep rupture and fatigue loading.

- For carbon-based FRP: 0.55 f_{ful}
- For glass-based FRP: 0.20 f_{ful}
- For aramid-based FRP: 0.30 f_{ful}

Where f_{ful} (ksi) is the design tensile strength of the FRP laminate in the longitudinal direction. The manufacturer's specified tensile strength is multiplied by an environmental reduction factor, C_E, to obtain the design tensile strength.

Table 3-5 Environmental reduction factors, CE, LRFD-FRP Section 2.6.1.2

Fiber Type	**C_E**	
	Normal environment	**Aggressive environment**
Glass	0.65	0.50
Carbon	0.85	0.85
Aramid	0.75	0.70

For glass-based FRP, these requirements effectively limit the maximum tensile stress in the FRP due to dead loads and a fatigue vehicle in each lane to 10% of the manufacturer's specified tensile strength. For the case of concrete structures that are reinforced with GFRP bars, ACI 440.01R15 limits the sustained tensile loading to 14% of the manufacturer's specified tensile strength. This limit is achieved through an environmental reduction factor of 0.7 for GFRP bars in concrete exposed to earth and weather and a creep/fatigue-rupture factor of 0.2.

3.1.2.4 Strength – Flexure

The basic design equation used to evaluate this limit state is found in AASHTO LRFD Section 3.

$$M_u \leq \phi . M_n$$

Where:

M_u : Factored moment demand
M_n : Nominal resistance
ϕ : Resistance factor

M_u, the factored moment demand, is found directly from Strength I Load Combination in Section 3 of AASHTO LRFD. M_n, the nominal resistance, is based on either concrete crushing failure mode or the maximum tensile stress in FRP exceeding the allowable limit.

The resistance factor, Φ, is found in LRFD-FRP Section 2.7.3.2. The value Φ can be determined as follow:

$\phi = 0.55$ if $\rho \leq \rho_b$
$\phi = 0.65$ if $\rho \geq 1.4\ \rho_b$
$\phi = 0.3 + 0.25.\frac{\rho}{\rho_b}$ if $\rho_b \leq \rho \leq 1.4\ \rho_b$

Where ρ_b is defined as the reinforcement ratio related to concrete crushing and FRP tensile rupture, and ρ is the cross-sectional area of the FRP tube to the cross-sectional area of the concrete core. The general concepts for these standards should be applicable to both the U-girder and DWB-36 alternatives even though they are originally established for CFFT sections (Brown, 2017).

3.1.2.5 Shear

The general design equation used to evaluate Limit State 4-b obtained from LRFD-FRP is:

$$V_u \leq \phi . V_n$$
$$V_n = V_c + V_{frp}$$

Where:
V_u : Factored shear demand
V_n : Nominal resistance
V_c : Shear resistance provided by concrete
V_{frp} : Shear resistance provided by FRP
ϕ : Resistance factor

AASHTO LRFD-FRP Section 2.7.3.2 states that the strength reduction factor for shear, Φ, is determined to be 0.75. Previous research on CFFT structural elements shows a lack of information on the shear behavior of FRP U-shaped girders.

3.1.3 FRP Material Properties Used in Current Study

Table 3-6 shows the different FRP composite material and their corresponding modulus of elasticity based on the fiber orientation. Using concrete to fill the girders increases the overall stiffness of the bridge and that results in less deflection; however, the down side of using such heavy material would increase the deal load which will have an effect on the creep and fatigue rupture. The steel modulus of elasticity can be on the order of 10 times greater than GFRP

Table 3-6 FRP composite material properties (*Brown, 2017*)

Fabric Type	Manufact.	ID	σ_{xx} (ksi)	σ_{yy} (ksi)	τ_{xy} (ksi)	E_{xx} (Msi)	E_{yy} (Msi)	Thickn./ layer (in.)
NCF 0/90 RI	VectorPly	E-LT-4400	73.8	74.2	13.1	3.9	3.92	0.044
NCF $0^{+}/90^{-}$ RI	VectorPly	E-LT-5500	120.4	46.6	13.1	6.57	2.44	0.054
NCF Carbon 0 RI	VectorPly	C-L 1800	198.7	4.2	7.9	16.56	1.43	0.024
Woven 0/90*	Hexcel	HexForce 1597	34.4	37.0	--	--	--	0.0378
Filament wound	WacoBoom	n/a	52.0	50.0	11.3	3.9	3.1	n/a
Pultruded carbon/ glass hybrid	Strongwell	n/a				5.76	1.69	n/a

Woven fabrics as shown in Figure # are used in many structural applications. Woven fabrics consists of a sequence of parallel yarns that run in the warp direction and an additional set of parallel yarns that run perpendicular in the weft direction. The wrap yarns go up and down the weft yarns that are woven from side to side. While weaving does achieve the desired goal of maintaining dimensional stability for the fibers.

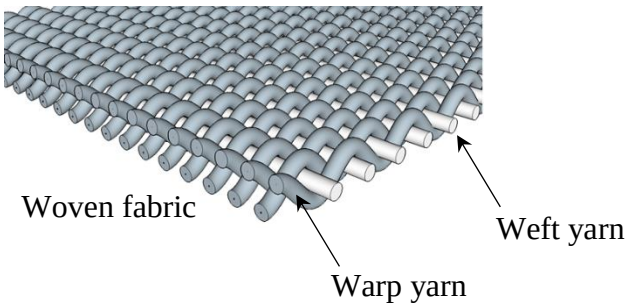

Figure 3-3 Woven Fabrics

In non-crimp fabrics, the warp yarn and weft yarns are kept straight as in two layers and held by multiaxial stitching fiber. The reason behind this is to maintain as much of the strength properties as in relation to uni-directional single-ply lamina.

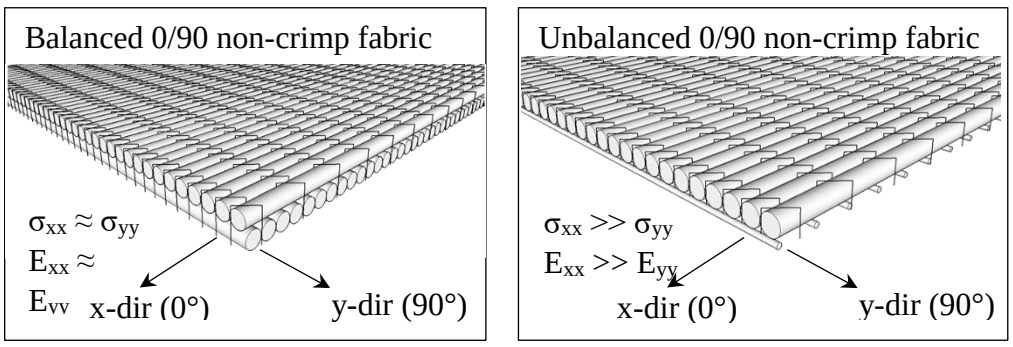

Figure 3-4 Non-crimp stitched fabrics

3.1.4 Span Length Evaluation

In the current study, span lengths of 30, 40, 50, 60, and 75 ft were evaluated for all three FRP alternatives. These span lengths have been considered as part of the so-called "span range gap". A pre-stressed Florida I-beam is capable to cover a span-length range of (80-200) feet in an extremely aggressive environment as shown in the figure below:

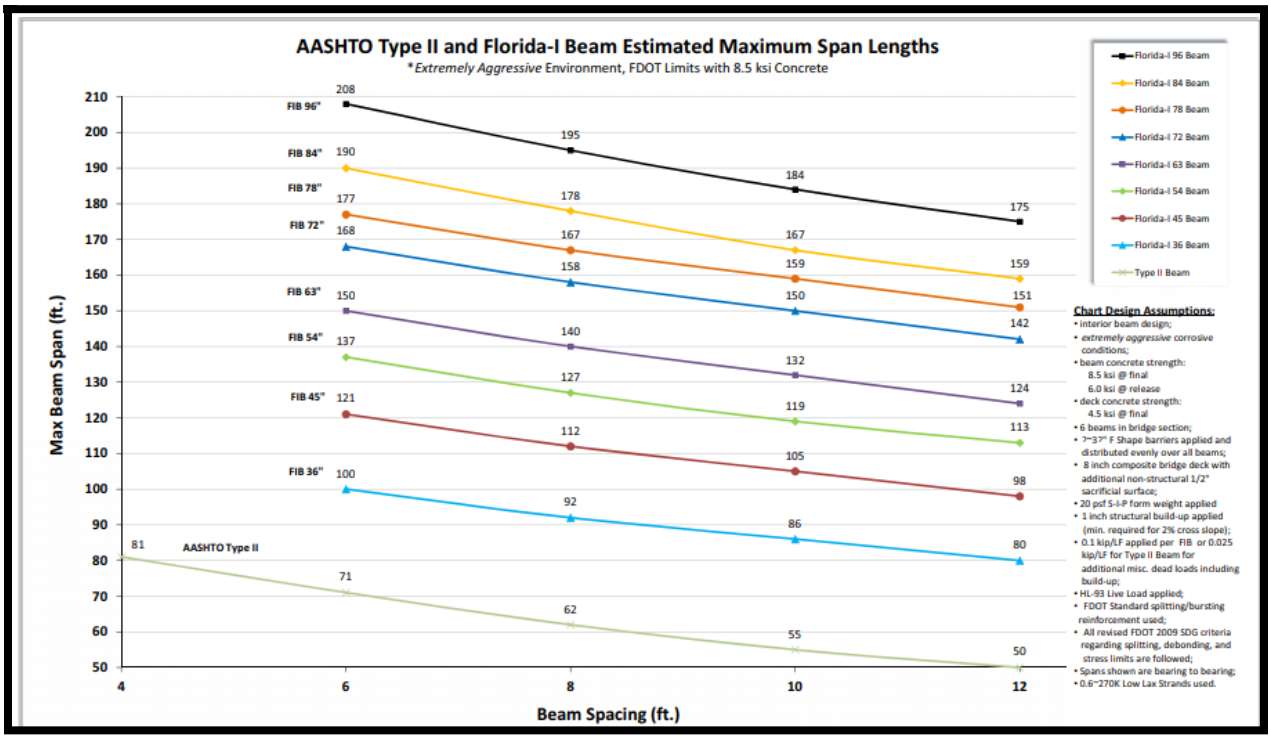

Figure 3-5 Maximum and minimum span-length for the pre-stressed Florida I-beam under extremely aggressive environment (FDOT, Index 20010, 2016)

3.2 Methodology

This phase of the research is originally a part of a research effort sponsored by the Florida Department of Transportation (FDOT). The work was completed by the Civil Engineering and Aerospace Engineering Departments at Embry-Riddle Aeronautical University (ERAU). Three bridge girder alternatives were chosen for analysis: hybrid FRP/concrete-filled U-girder, hybrid

FRP/concrete-filled tube, and a pultruded double-web I-beam (DWB). These alternatives were selected based on a comprehensive survey as part of the FDOT project for in-service FRP-girder bridges in the U.S. along with several projects in Europe.

3.2.1 Pultruded Double-Web I-beam (DWB)

The first alternative was the pultruded double-web I-beam (DWB). Strongwell has developed two unique cross-sections 8" x 6" EXTREN DWB Hybrid and 36" x 18" EXTREN DWB Hybrid. The DWB section is manufactured using the pultrusion process.

Strongwell provides the pultrusion manufacturing method for supplying continuous lengths of reinforced polymer with constant cross-sections. Raw materials are a liquid resin and flexible reinforcing fibers. The 8"x 6" EXTREN DWB - H (8" DWB-H) beam consists of four different types of glass fiber in the webs while the top and bottom flanges consist of carbon-fiber.

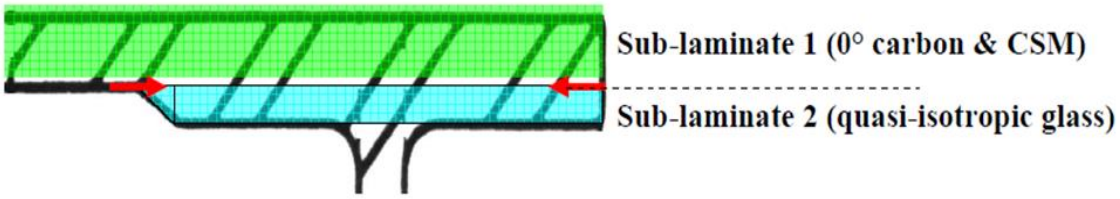

Figure 3-6 Part of DWB cross-section that shows the interface between the carbon fiber and fiber glass in the area between the web and flange (Cousins, 2005)

The carbon tows and glass rovings are bonded together using a vinyl ester resin matrix. The effective modulus of elasticity of the EXTREN DWB is improved by at least 30% when using carbon tows in the flanges. The fiber (glass and carbon) volume fraction is roughly 55%, and the beam's weight is 11.2 pounds per linear foot. The 36" x 18" EXTREN DWB BEAM — HYBRID BEAM is an identical version of the 8" DWB-H except it weighs 70 pounds per linear foot and has a total depth of 36 inches (Strongwell, 2003).

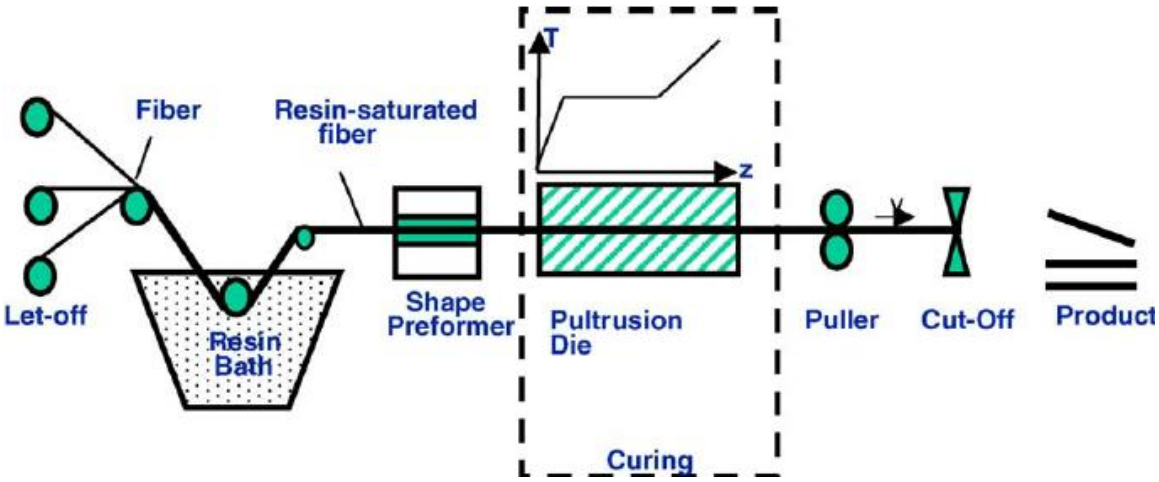

Figure 3-7 Pultrusion process (Acquah, 2006)

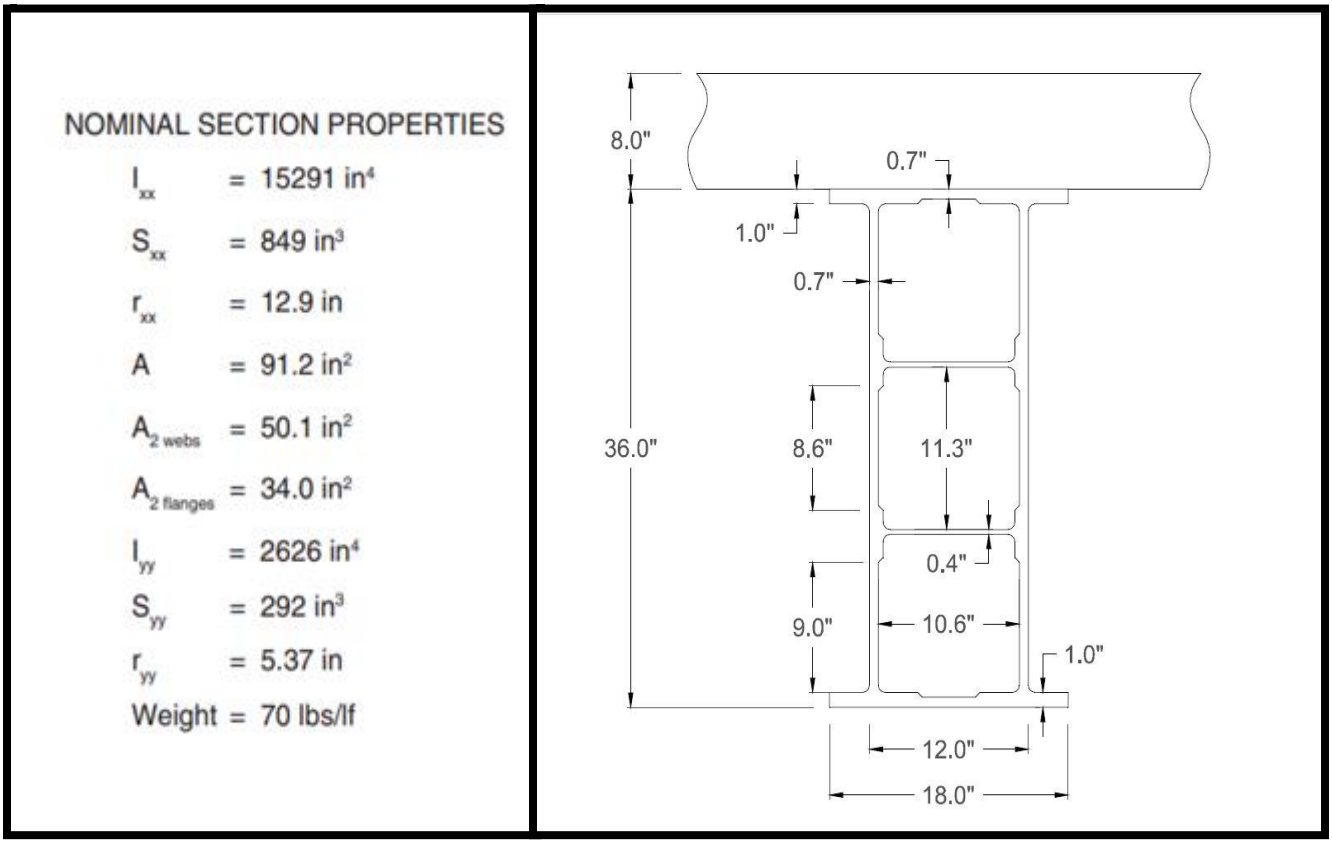

Figure 3-8 Cross-section of the 36" x 18" EXTREN DWB Beam and its nominal section properties (Strongwell, 2003).

3.2.1.1 Finite Element Analysis (FEA)

In the current study, design analysis software, ANSYS, was used to evaluate the limit states for EXTREN DWB-36 beams. The geometry of the DWB was fixed because the manufacturer, Strongwell, only provides two unique cross-sections. The Finite Element Modeling (FEM) method was used to evaluate four limit states: concrete compressive stress, deflection, fatigue/creep-flexure, and strength (flexure and shear). Full composite action between the FRP beams and RC deck was assumed in this study.

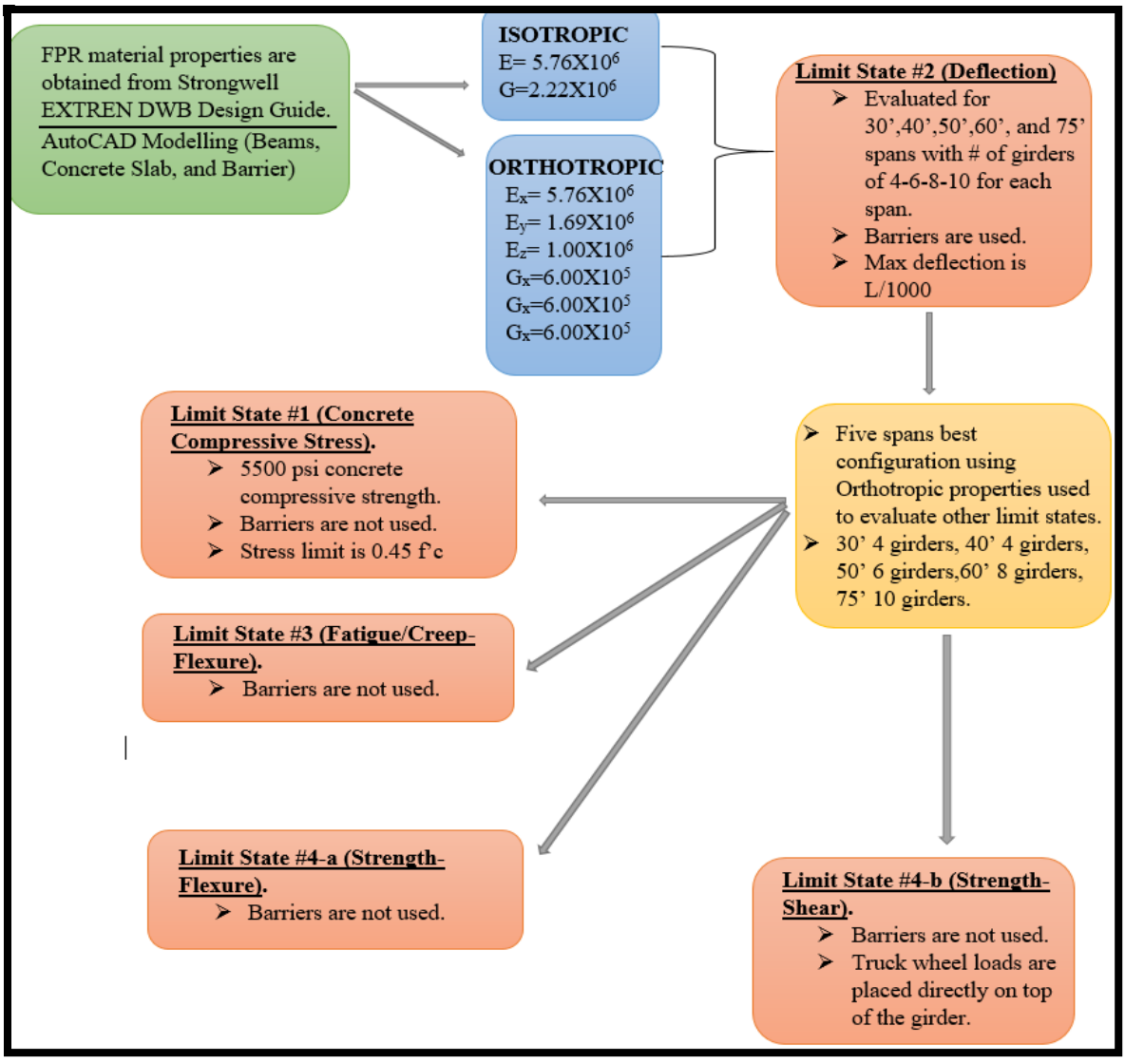

Figure 3-9 General analysis and design framework for DWB beams

3.2.1.1.1 3D-Model

AutoCAD 3D was used to create the actual bridge model, beams, deck, and barriers. The deck was modeled using solid elements while the beams were modeled as surfaces using shell elements. The shell elements are more efficient from a computational perspective and reduce the overall time required to run the simulation.

Figure 3-10 Bridge AutoCAD 3D model

3.2.1.1.2 Material Properties

Material properties were specified for the deck and the beams. The material properties for the deck were not changed during the entire study. Isotropic and orthotropic material properties

Table 3-8 FRP properties using Orthotropic Elasticity

Properties	Value	Unit
Density	105	lb ft^-3
Young's Modulus X Direction	5.76E+06	psi
Young's Modulus Y Direction	1.69E+06	psi
Young's Modulus Z Direction	1.00E+06	psi
Poisson's Ratio XY	0.3	
Poisson's Ratio YZ	0.3	
Poisson's Ratio XZ	0.3	
Shear Modulus XY	6.00E+05	psi
Shear Modulus YZ	6.00E+05	psi
Shear Modulus XZ	6.00E+05	psi

Table 3-7 FRP properties using Isotropic Elasticity

Properties	Value	Unit
Density	105	lb ft^-3
Young's Modulus X Direction	5.76E+06	psi
Young's Modulus Y Direction	5.76E+06	psi
Young's Modulus Z Direction	5.76E+06	psi
Poisson's Ratio XY	0.3	
Poisson's Ratio YZ	0.3	
Poisson's Ratio XZ	0.3	
Shear Modulus XY	2.22E+06	psi
Shear Modulus YZ	2.22E+06	psi
Shear Modulus XZ	2.22E+06	psi

were utilized for the beams to illustrate how the fiber orientation and shear deformation impact the overall bridge stiffness.

Table 3-9 Reinforced concrete properties

Properties	Value	Unit
Density	150	lb ft^-3
Young's Modulus	4.51E+06	psi
Poisson's Ratio	0.3	

3.2.1.1.3 Composite Action and Mesh Size

After creating the model using AutoCAD 3D, the model was saved in a format that can be used in ANSYS workbench for analysis. ANSYS 17.0 workbench was used to evaluate four limit states for the 36" x 18" EXTREN DWB Hybrid bridge. Composite action was established between the concrete slab and the FRP beams using bonded contact features as shown in the figure below.

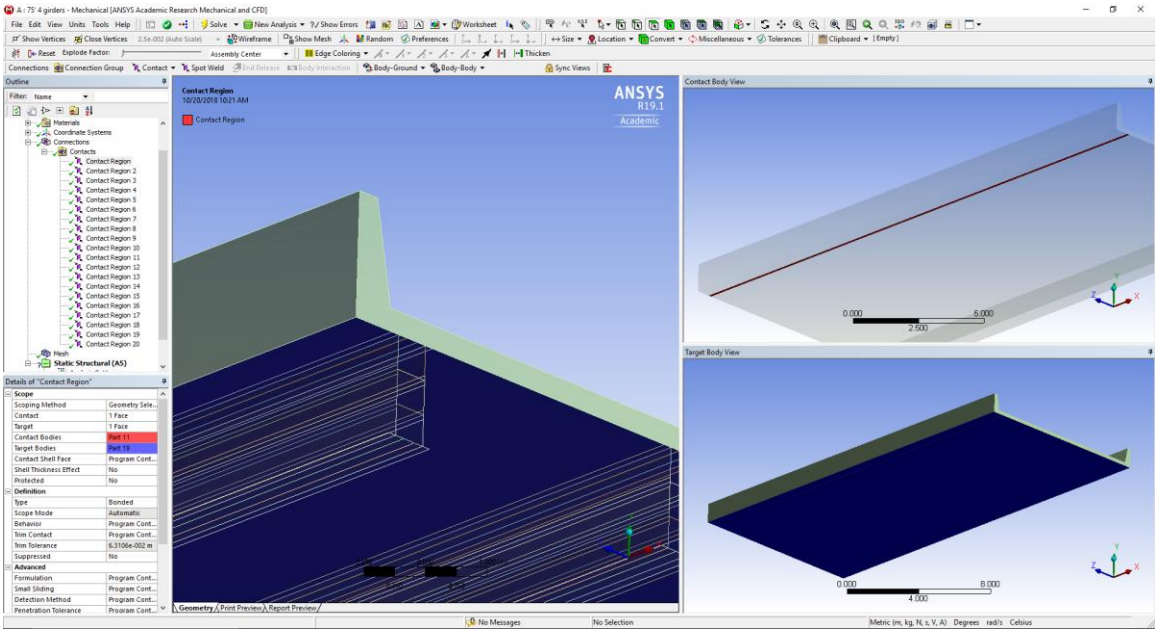

Figure 3-11 Composite action between the reinforced concrete slab and the FRP beams using bonded contact

Table 3-10 FEM element size analysis

Max. Element Size (in.)	# of Elements	Max. Deflection (in.)	Max. Compressive Stress (psi)
Default	22752	0.814	-575.3
12	22576	0.814	-585.43
10	28558	0.815	-587.93
8	37692	0.816	-586.26
6	67946	0.820	-589.06
4	155092	0.821	-589.28

3.2.1.1.4 Loads Cases and Loads Locations

The AASHTO HL-93 design truck/tandem was used in the FEA. In order to position the truck where the maximum loading is generated, shear and moment envelopes were generated for each limit state.

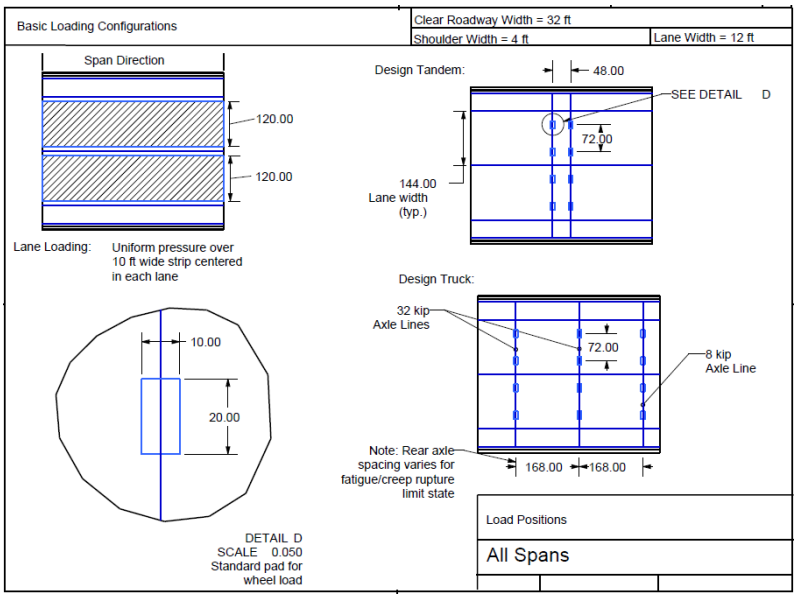

Figure 3-12 Basic loading configurations (*Brown, 2017*)

Each limit state has a special loading configuration. For truck loads and tandem wheel loads, a concentrated force equivalent to the appropriate wheel load was applied to a 10”x20” surface area in accordance with LRFD-7. Pressure loads were used to represent lane live load and barrier self-weight.

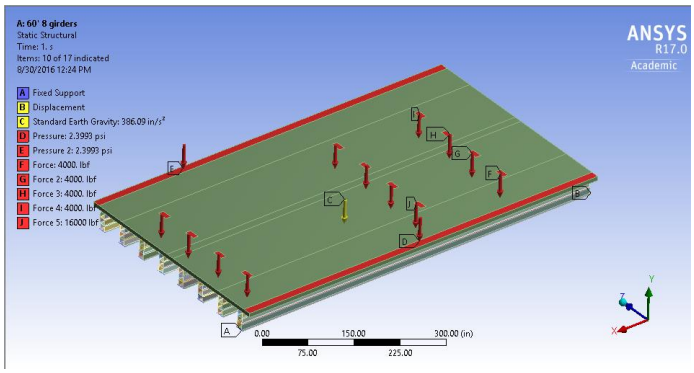

Figure 3-13 shows the tuck wheel loadings as pressure rectangles

3.2.1.1.5 Boundary Conditions

The bridge was assumed to be simply supported. A pin support was created at the bottom edge of all girders on one end of the bridge while on the other end a rolling support was established where the movement is free along the x-axis only.

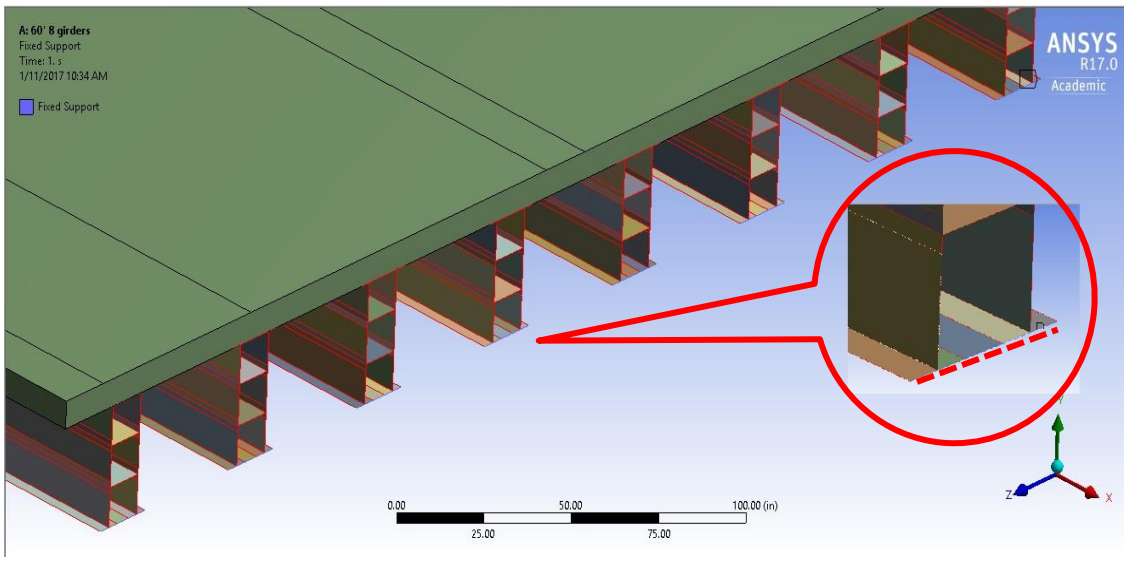

Figure 3-14 Bridge support locations

3.2.1.2 Results and Discussion

3.2.1.2.1 Deflection

Previous studies have shown that deflection is the controlling limit state when investigating the DWB bridge girders. In the current study, deflection was also assumed to be the controlling limit state. The deflection of the bridge was limited to L/1000. For deflection, both the isotropic and the orthotropic material properties were investigated. Barriers on each side of the bridge were included only when evaluating deflection. Only the live load was included to evaluate this limit state.

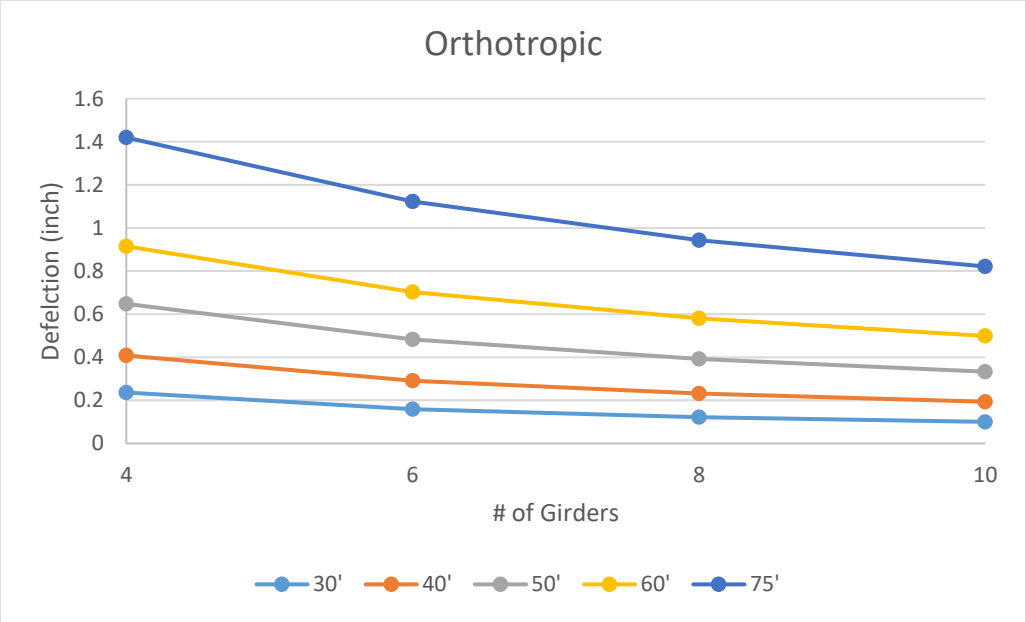

Figure 3-15 Result for deflection using orthotropic material properties

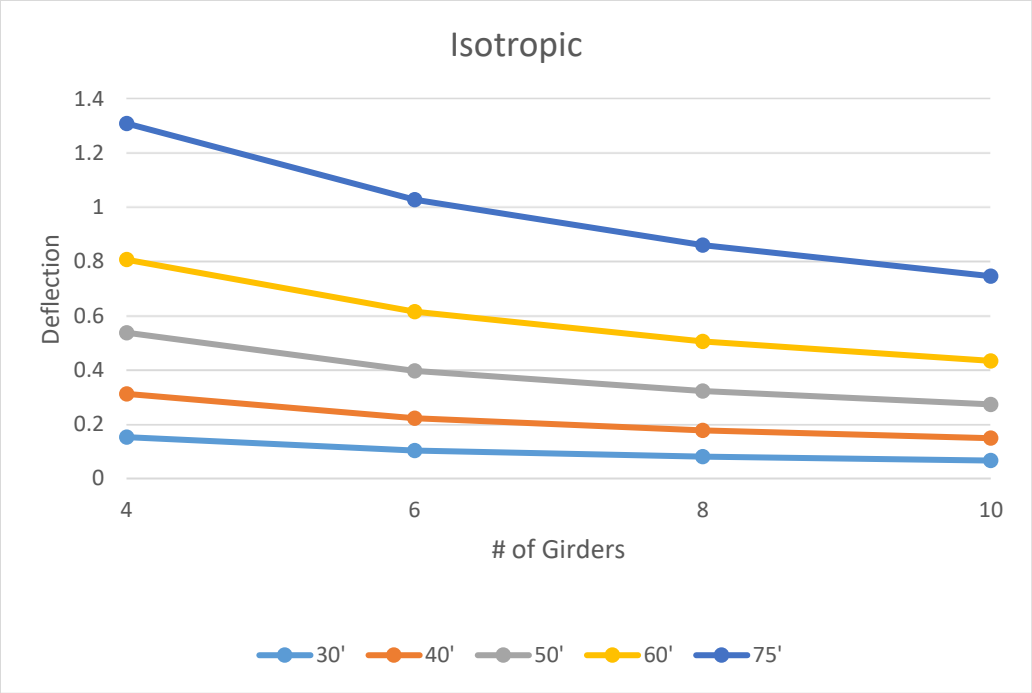

Figure 3-16 Result for deflection using isotropic material properties

Table 3-11 Orthotropic deflection result for all span lengths

Span (ft.)	**Allowable (in.)**	**Number of Girders**			
		10	***8***	***6***	***4***
30	0.36	0.1	0.12	0.16	0.24
40	0.48	0.19	0.23	0.29	0.41
50	0.6	0.33	0.39	0.48	0.65
60	0.72	0.5	0.58	0.7	0.92
75	0.9	0.82	0.94	1.12	1.42

The result from the orthotropic case are taken into consideration because they accurately represent a real-world scenario. The numbers that are highlighted in red correspond to deflections that meet the L/1000 criteria. The number of girders that correspond to these deflection values are used to evaluate the remaining limit states.

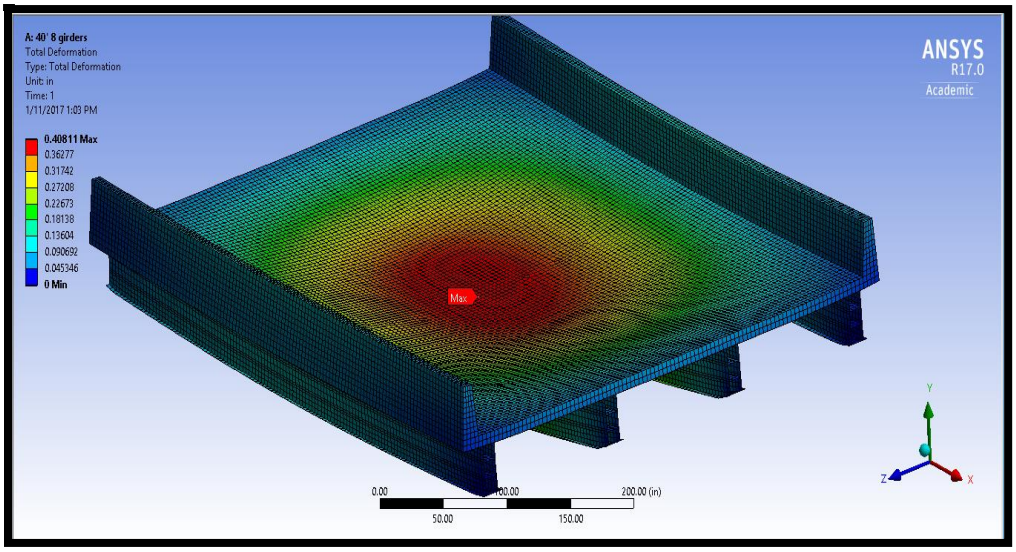

Figure 3-17 Maximum deflection for the 40-ft span using orthotropic material properties

3.2.1.2.2 Concrete Compressive Stress

For this limit state, the maximum concrete compressive stress was assumed to be 0.45 X 5500 psi. The tandem wheel loads, lane live load, barrier self-weight, and girder and slab self-weight were all applied to evaluate the concrete compressive stress on 8-in thick concrete slab.

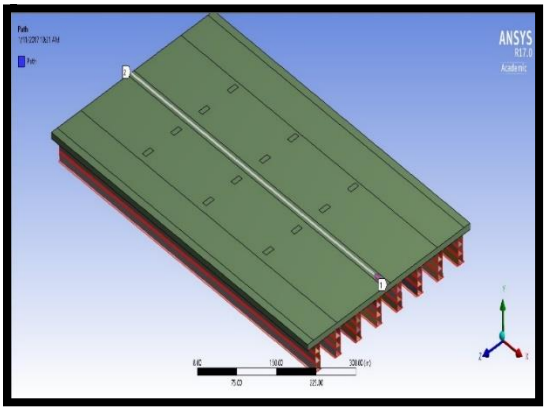

Figure 3-19 Path created on the top surface of the concrete to evaluate the concrete compressive stress

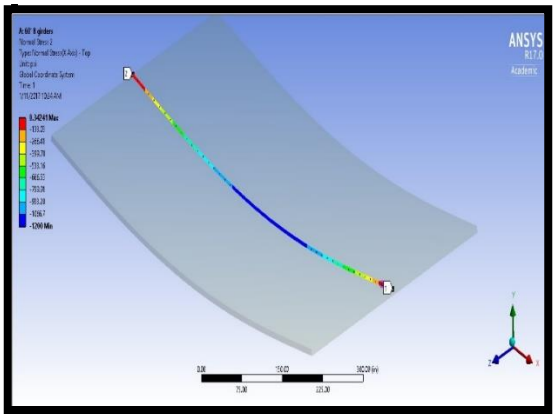

Figure 3-18 Result of the normal stress along the path

A longitudinal path was created along the entire bridge to show the stresses on the top surface of the slab where the bridge experienced the highest concrete compressive stress. As the

span length increases, the normal compressive stress increases. The allowable concrete compressive stress is 0.45x5500 psi = 2475psi. The compressive stress results from the FEA do not exceed the maximum compressive stress for all span lengths.

Table 3-12 Maximum normal stresses for all span lengths

Span (ft.)	# of Girders	0.45 f'c 0.45x5500 (psi)	Max. Normal Stress (psi)
30	4	-2475	-920.8
40	4	-2475	-1207.6
50	6	-2475	-1144
60	8	-2475	-1303.8
75	10	-2475	-1620.7

3.2.1.2.3 Fatigue/Creep – Flexure

In this limit state, a fatigue-modified design truck, concrete deck, girder self-weight, and 15 psf (73 kg/m^2) future wearing surface are included to evaluate the maximum tensile stress on the bridge girders. The red arrows (Figure 3-18) represent the design truck wheels, and the yellow arrow represents the self-weight of deck and girders. The barriers dead load was represented as pressure over a 15 inches (381 mm) strip. The future wearing surface pressure was applied on the area between the barriers.

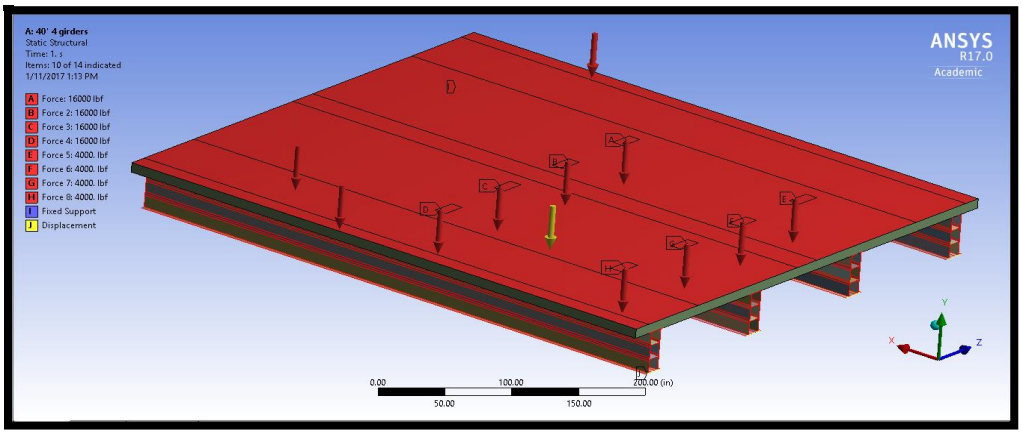

Figure 3-20 Loading condition for limit state-3

The maximum tensile stress is located at the bottom flange. A line of stresses along the entire bottom flange of the interior girder was separated as shown in the figure below.

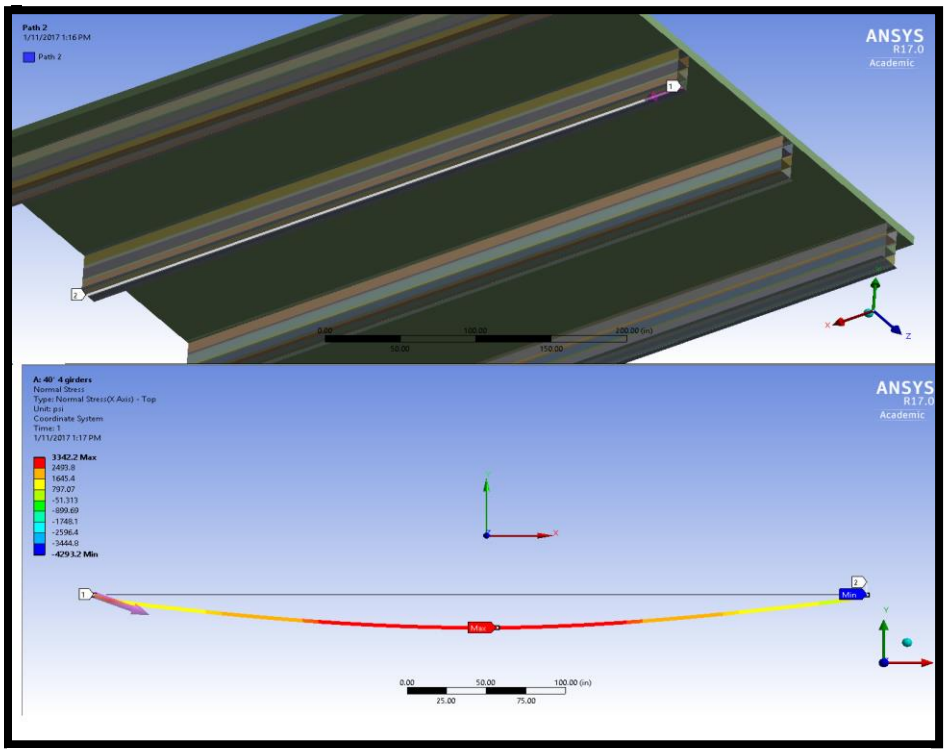

Figure 3-21 Stresses along the bottom flange of the FRP girder

Table 3-13 Fatigue/Creep – Flexure Result

Span(ft)	Max. Normal Stress (psi)
30	2113.5
40	3347.5
50	3322.2
60	3484.2
75	4396.7

3.2.1.3 Girder Distribution Factor for DWB

A thesis was completed by Restrepo at Virginia State University evaluating the Rt. 601 Bridge using field testing to determine girder distribution factors (GDF) for bending moment. In

this bridge, 36-inch DWBs were used to support a laminated timber deck. The bridge was tested in the field using dump trucks. Two field tests were performed over a two-year period in 2001 and 2002. The deflection and strain results were used to calculate the distribution factor. During the preliminary design of the bridge, Timoshenko's Shear Deformable Theory was used to derive an equation that takes into account the shear stiffness of the material when calculating the deflection as shown below (Restrepo, 2002).

$$\Delta_{ms.} = \frac{pa(3L^2 - 4a^2)}{48EI} + \frac{pa}{2kGA}$$

Where: p = Load (kip)
E= Elastic Modulus (Ksi)
I = Moment of Inertia (in^4)
L= Length of Beam (in.)
kGA= Effective Shear Stiffness (ksi-in^4)
a = Distance load applied from end (in.)
$a \leq L/2$

In the current study, reliability analysis tools and AASHTO-LRDF Bridge Design were used to verify the results for the GDF for the Rt. 601 Bridge. A Monte-Carlo Simulation was used to calculate the reliability index for the DWB bridge girders. In order to use the Monte-Carlo Simulation, load and resistance models must be determined.

3.2.1.3.1 Load and Resistance Models

The load model in this analysis was considered to be a simply supported beam with multiple concentrated load points representing the design truck wheels. The modulus of elasticity of the hybrid DWB beam is the combined modulus of elasticity of both the glass fiber in the web and the carbon fiber in the flanges. The equation used in the load model was the same equation that was derived by Virginia State University after performing a four-point bending test on the

girders to determine the modulus of elasticity and the shear stiffness using Bernoulli/Euler theory.

The statistical properties of the Young's modulus of the hybrid DWB shows a mean of 6.46 Msi. A standard deviation of 0.19 as has been suggested by some studies (Virginia Polytechnic and State University, 2002). The same studies show the mean and standard deviation for the shear stiffness modulus are 47.59 Msi-in and 8.84 respectively. These values for the Young's modulus do not change with time, so only one set of data would be needed (Schniepp, 2002). Using AASHTO LRFD Bridge Design Specification for deflection limitation for service live load, the deflection limit was L/800 when evaluating the GDFs.

Table 3-14 Variables and their means and standard deviation

Type	Variable	Deterministic	Mean (Unit)	Std.
/	Eb	/	6.46 (Msi)	0.19
Material Properties	Ew	/	1.76 (Msi)	0.22
/	Ec	/	3.83 (Msi)	0.22
/	kGA	/	47.59 (Msi-in)	8.84
Geometry	/	L	/	/
/	/	I	/	/
Live Load	P	/	90 (Kips)	0.01

3.2.1.3.1 GDF Calculation Using AASHTO-LRFD

	Value	Unit
A	91.2	in2
I	15291	in^4
Eb	6000	ksi
Ed	1754.96	ksi
S	3.5	ft
L	39	ft
ts	5.13	in
eg	20.56	in

$$n = \frac{Eb}{Ed} = 3.42$$

Kg= $n(I + Aeg^2)$= 184081.1

g= $0.075+(\frac{S}{9.5})^{0.6} * (\frac{S}{L})^{0.2} * (\frac{Kg}{12\ L\ t_s^3})^{0.1}$ = 0.453

$\frac{g}{wheel\ line}$ = 0.452551/2 = 0.226

A = Area of the girder cross section

I = Moment inertia

Eb = Modulus of elasticity of beam

Ed = Modulus of elasticity of deck

S = Spacing of supporting components

L = Span length of beam

ts = Depth of slab

eg = Distance between centers of gravity of the beam and deck

3.2.1.3.2 Deflection Calculation

To find the location of the resultant *Fr*, the sum of moments around any of the wheel loading must be taken. In this case, the sum of moments was taken at the wheel loading of 14.20 kips (45 kN). The maximum moment occurs when *Fr* is 221.66 inches (5.6 m) away from R_a. This distance and value for *Fr* would be used to find the maximum deflection of the bridge at this location of the truck.

20.58 kips *14.67' +20.58 kips*19.125'= (14.20+20.56+20.56)kips *(14.67-x)
solve for x
x=2.07'=24.84"

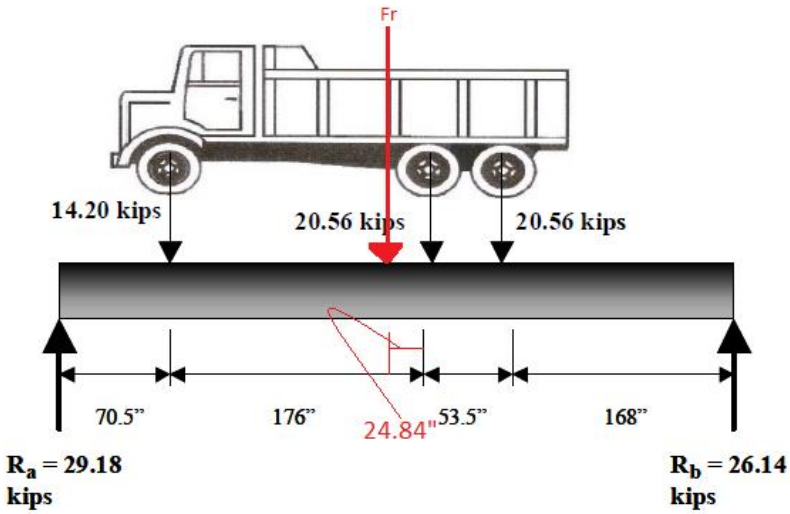

Figure 3-22 Location of the truck load resultant to produce maximum moment

In order to find the deflection for each interior girder, the calculated deflection need to be multiplied by the GDF. Virginia Tech calculated the GDF per wheel line. They divided the total GDF by two because there are two wheel lines per truck.

3.2.1.3.3 Reliability Index Calculation Using Monte-Carlo Simulation

$$G = R - Q$$

$$Q = \left[\frac{pa(3L^2-4a^2)}{48EI} + \frac{pa}{2kGA}\right] * \left[0.075 + \left(\frac{S}{9.5}\right)^{0.6} * \left(\frac{S}{L}\right)^{0.2} * \left(\frac{\frac{Eb}{Ed}(I+Aeg^2)}{12\,L\,t_s^3}\right)^{0.1}\right]$$

	value	Unit
p	55.2	kips
I	15291	in^4
a	221.66	in
E	6460	Ksi
L	468	in
kGA	47590	Ksi-in^2

$$\Delta ms = \frac{pa(3L^2-4a^2)}{48EI} + \frac{pa}{2kGA} = 1.317 \text{ in.}$$

$\Delta ms = 1.31701 * GDF$=1.31701*0.226275 = 0.298 in.

$$R = L/800$$

R: Resistance model

Q: Load model

After determining the load and resistance models, a Monte-Carlo simulation was used to analyze the probability of exceeding the deflection criteria. The load model equation consists of the deflection and GDF equations. Variables were chosen based on the availability of studies of the statistical data of these variables. Moment of inertia of the DWB, the span length, and the girder spacing are selected to be deterministic. All variables are normally distributed. An excel spreadsheet was used to generate the Monte-Carlo simulation.

$$\beta = \frac{\mu_R - \mu_Q}{\sqrt{\sigma_R^2 + \sigma_Q^2}}$$

Where β is the reliability index, μ_R, μ_Q are the means of the resistance and load models, and σ_R, σ_Q are the standard deviations for the resistance and load models. 1000 iterations were required for the Monte-Carlo simulation for the β value to converge.

3.2.1.3.4 Results and Discussion

To compare the findings from the field test and the calculated deflection, the maximum deflections were only compared with the results of the east and west interior girders. The maximum deflection from the field test was 0.242 inches (6.1 mm) at G#3 on the west side of the bridge using a GDF of 0.235. The calculated deflection was found to be 0.298 inches (7.6 mm) using a GDF of 0.226. There is a **24**% of difference between the calculated deflection and the deflection that was measured on the field; however, the calculated deflection value is higher, which makes it more conservative. A $\boldsymbol{\beta}$ of 1.84 was calculated for the deflection limit state for the Virginia Route 601bridge. This reliability index value is equivalent to the probability of failure of $\rho_f = 0.0329 \approx \frac{1}{30}$. Since deflection is considered to be a service limit state, this likelihood of exceeding L/800 is acceptable.

The same models were used to evaluate the probability of failure for the FEM with a concrete deck instead of timber. The resistance model used is more conservative (L/1000) compared to resistance model that was used in the Virginia Route 601 Bridge. Monte-Carlo simulation was used to generate a set of $\boldsymbol{\beta}$ values based on different span lengths and different girder spacing.

Table 3-15 Probability of failure for different span length

Span Length (ft)	β	ρ_f	# girder
30	10.27	0	3
40	7.78	$3.63x10^{-15}$	4
50	4.91	$4.55x10^{-7}$	5
60	2.70	$3.47x10^{-3}$	6
75	0.5	$3.09x10^{-1}$	8

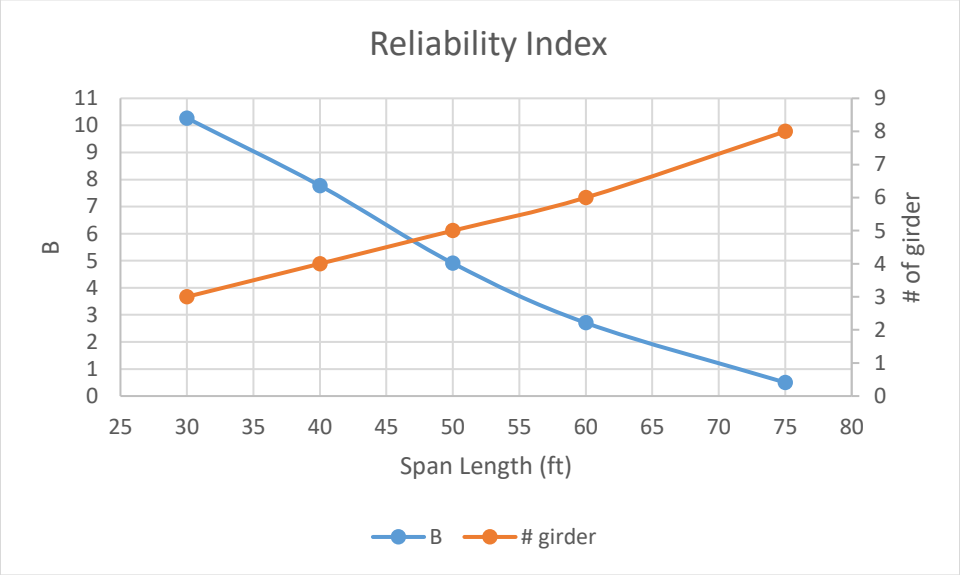

Figure 3-23 Reliability indices with respect to the span length and the girder spacing

Table 3-16 Number of girder using Finite Element Modeling versus using the probability analysis

Span Length(ft)	# of Girders	
	FEM	β
30	4	3
40	4	4
50	6	5
60	8	6
75	10	8

After analyzing the probability of failure, the number of girders have been reduced for each span length. No previous failure analysis has been completed for an FRP bridge girder, so there is no target reliability to be used as a design factor. The figure above shows that only three girders are needed for the 30 ft (9.1 m) span with zero probability of failure. As the span length increases, the girder spacing decreases and the probability of failure increases.

3.2.2 Hybrid FRP/Concrete-Filled U-Girder

The second alternative was the hybrid FRP/concrete-filled U-girder. A common manufacturing method to fabricate the U-shaped girders is the hand lay-up method. Another method that was used to manufacture the Refugio County girders is the vacuum assisted resin transfer molding (VARTM) or vacuum infusion processing (VIP). An optimization study was completed by Papapetrou (2017), a PhD. student at ERAU, on similar U-shaped FRP girders that were constructed in Poland and Texas. Finite Element Analysis (FEA) was used to evaluate all applicable limit states (LS).

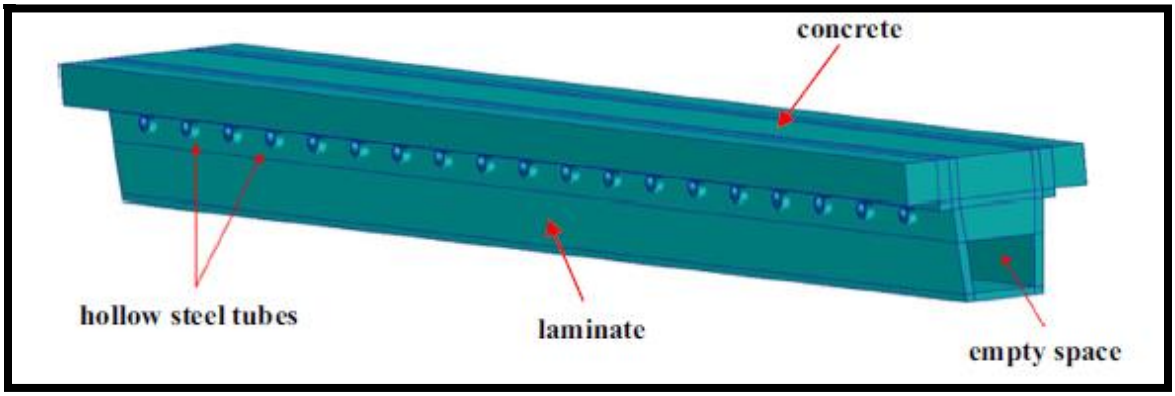

Figure 3-24 U-shaped girder with 8" reinforced concrete slab on top (*Papapetrou, 2017*).

The main objective of the optimization was to reduce the FRP material used in a U-girder while still maintaining the required strength. The AASHTO distribution factor method was not used in the optimization approach, and the entire bridge was modeled. The optimization variables were the size and shape of the girders. In the optimization result, having cross-sections with equal side and base thicknesses, due to manufacturing constraints, does not result in lightweight designs.

3.2.2.1 Results Summary

In order to determine the girder depth that results in the least cost, the cost of the concrete that is used to fill the FRP U-girder must also be considered. In the current study, an FRP cost of $5.25 per pound and a cast-in-place concrete cost of $0.21 per pound is assumed (Performance Composites). After the total concrete and FRP costs are considered for all of the girders in a specific configuration (not including the concrete in the slab), a more traditional series of optimization curves is obtained. Unlike the curves representing total FRP weight, the total cost

curves now increase as the girder depth becomes large due to the additional cost of the concrete required to fill the girders (Brown, 2018).

3.2.3 Hybrid FRP Concrete-Filled Tube

The third alternative was the concrete filled FRP tube (CFFT). This type of bridge girder is commonly used in Concrete Arch Bridge System (CABS, formerly known as "Bridge-in-a-

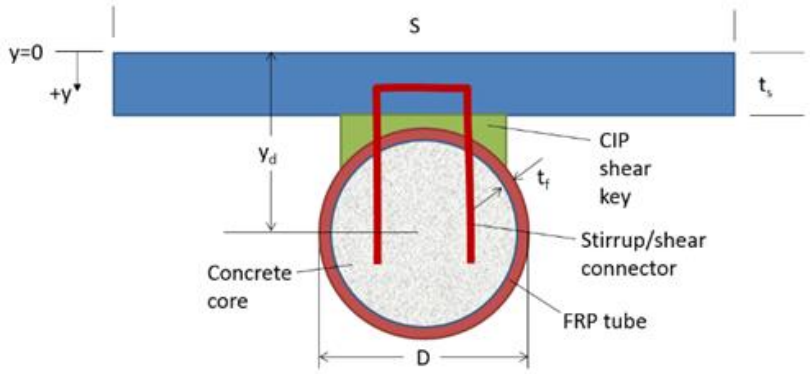

Figure 3-25 Cross-section of CFFT shows the design parameters (*Brown, 2017*)

Backpack"). Filament winding is one of the methods used to fabricate CFFT. An optimization study for the CFFT was completed by the Civil Engineering Department at ERAU. The AASHTO Distribution Factor method was used in the optimization process to determine the minimum FRP thickness required to fulfill each limit state.

3.2.3.1 Results and Discussion

The Figure below shows the final result for the optimization process. Number of FRP girders were chosen to be N_b=6 and N_b=8 for the final comparison. The optimization results conclude that the circular tube is not the most effective structural shape when it comes to shear or resisting bending moment. When composite action is present between the CFFT and the RC deck, more of

the composite will not experience large stresses because it will be close to the neutral axis (Brown, 2017).

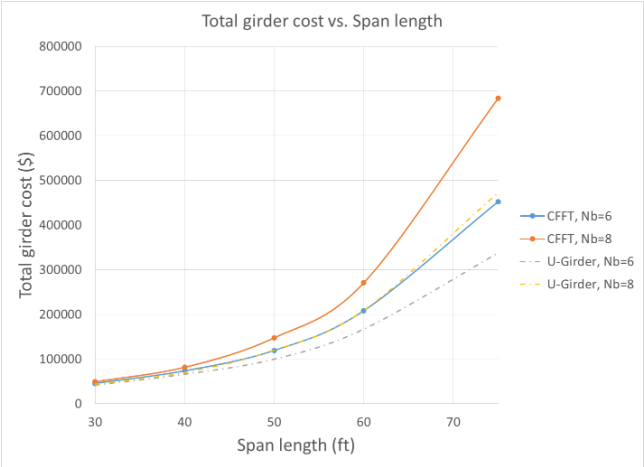

Figure 3-26 Cost analysis for the optimal values for CFFT bridge girders using the AASHTO distribution factor method (*Brown, 2017*)

3.3 Results Summary

After combining the result from the current study and the results from the study that was completed by the Civil Engineering Department at ERAU sponsored by the FDOT, a comparison was made to select the best FRP alternative. The structural analysis and results of this study can be used as a foundation for future research. A final cost analysis was completed by the Civil Engineering Department for the three alternatives. The results for the U-girder and CFFTs were based on a six-girder bridge with the assumption of a 100% stiffness contribution by the concrete beneath the slab for the U-girders. As shown the Figures below, as the span length increases, the difference between the U-girder and the other two alternatives becomes more distinct.

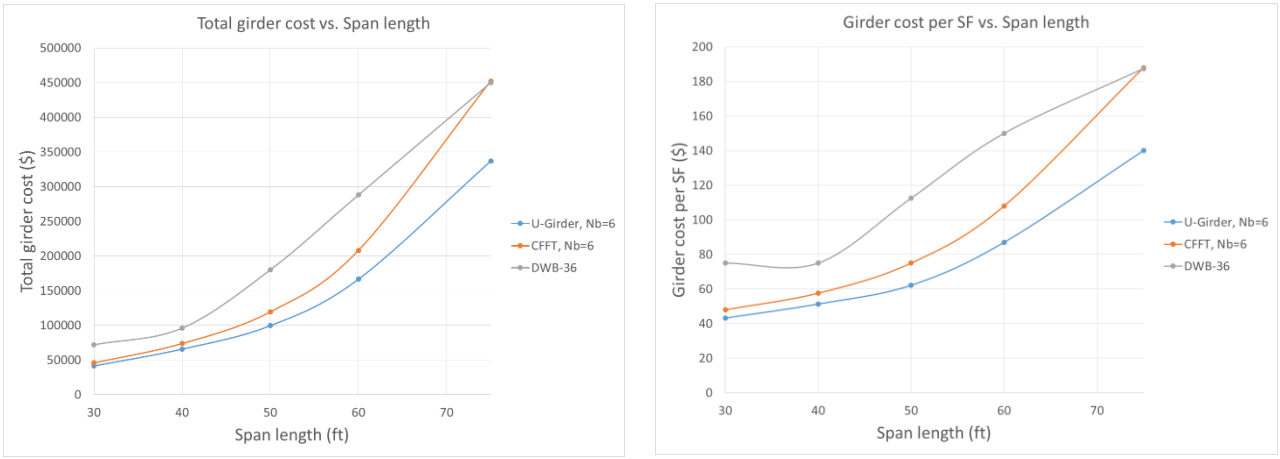

Figure 3-27 Cost analysis for the U-girders, CFFT, and DWB-36 (*Brown, 2018*)

Chapter 4 Vacuum Infusion Processing for FRP Panels

4.1 Background

Fiberglass, carbon fiber (graphite), Kevlar, quartz and polyester are fibers used to formulate a typical composite material. The fibers come in different structures such as veil mat, short fibers mat, woven cloth, unidirectional tape, biaxial cloth or triaxial cloth. The resins that hold the fibers together are usually thermoset resins such as epoxy, polyester, vinyl ester, polyurethane and phenolic. Fiber- weight fractions typically vary between 40% and 70% depending on the type of manufacturing process used. With higher fiber content and continuous fibers, better strength and stiffness is guaranteed (Performance Composites, unknown)

Typical glass fibers are divided into two categories: - low-cost general-purpose fibers and premium special-purpose fibers. The general-purpose products are called E-glass, and they makeup over 90% of all glass fibers produced that are subject to ASTM specifications. The remaining glass fibers are premium special-purpose products. Not all glass fibers are subject to ASTM specifications. Each of those glass fibers has a letter designation indicating unique properties. (Wallenberger, 2001).

Letter designation	Property or characteristic
E, electrical	Low electrical conductivity
S, strength	High strength
C, chemical	High chemical durability
M, modulus	High stiffness
A, alkali	High alkali or soda lime glass
D, dielectric	Low dielectric constant

4.2 Basic Material Properties

Glass-fiber material properties vary based on fiber orientation, type of resin, fiber to resin ratio, and temperature. There was not any data sheet can be found for the 600 g/sq.m

unidirectional fiber glass; however, a data sheet for 525 g/sq.m was used as a reference to evaluate the test results. The purpose behind this experiment is to demonstrate if 0.7" in thickness FRP beam can be built using Vacuum Infusion Process method (VIP), and if it was feasible, what the difficulties would be.

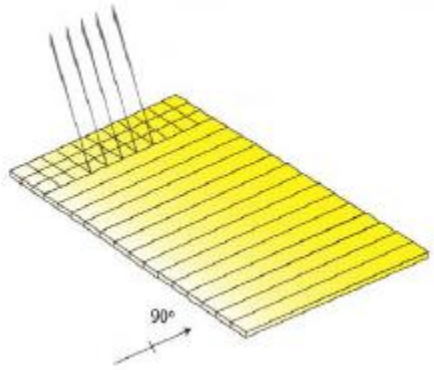

E-T 1600

Fiber Type: E-Glass
Architecture: 90 Weft Unidirectional
Dry Thickness: 0.031 in. / 0.79 mm
Total Weight: 15.49 oz/sq.yd / 525 g/sq.m

Laminated Properties 0 °

Laminate Weight		E-T 1600 Resin Infused
Fiber	0.11 lb/sq.ft	0.53 kg/sq.m
Resin	0.05 lb/sq.ft	0.23 kg/sq.m
Total	0.15 lb/sq.ft	0.75 kg/sq.m

Physical Properties		E-T 1600 Resin Infused
Density	1.10 oz/cu.in	1.90 g/cc
Fiber Content	70% by Wt.	52% by Vol.
Thickness	0.016 in	0.4 mm

Laminate Modulii		E-T 1600 Resin Infused
Ex	2.08 MSI	14.35 GPa
Ey	5.70 MSI	39.30 GPa
Gxy	0.66 MSI	4.53 GPa
Ex,flex.	1.98 MSI	13.64 GPa
Ey,flex.	5.41 MSI	37.33 GPa

Ultimate Stress		E-T 1600 Resin Infused
Long. Ten.	20.8 KSI	143.5 MPa
Long. Comp.	20.8 KSI	143.5 MPa
Trans. Ten.	107.9 KSI	744.0 MPa
Trans. Comp.	107.9 KSI	744.0 MPa
In-Plane Shear	13.1 KSI	90.6 MPa
Long. Flex.	19.8 KSI	136.4 MPa
Trans. Flex.	128.8 KSI	888.0 MPa

Figure 4-1 525 g/sq.m unidirectional non-crimp glass-fiber material properties (*Vectorply, 2015*)

Table 4-1 Cost and material properties comparison for fiberglass, wood, aluminum, and steel (Performance Composites)

	Fiberglass & polyester	Graphite & epoxy	Wood (Douglas fir)	Aluminum Sheets 6061 T-6	Steel Sheets
Material Cost $/lb	$2.00-3.00	$9.00-20.00+	$0.80	$4.50-10.00	$.50-1.00
Strength, yield (psi)	30,000	60,000	2,400	35,000	60,000
Stiffness (psi)	1.2×10^6	8×10^6	1.8×10^6	10×10^6	30×10^6
Density (lb/in^3)	.055	.065	.02	.10	.30

In the current study, Fibre Glast #1110 vinyl ester resin and methyl ethyl ketone peroxide (MEKP) hardener were used. #1110 Vinyl Ester resin properties are corrosion resistance, heat resistant, and blended for toughness. #1110 vinyl ester resin can be used to repair tank linings, blisters in boat hulls, and fabricate tough all-around parts. It is an excellent for resin infusion applications because it has a low viscosity (Fibre Glast, 2018).

Table 4-2 #1110 Vinyl Ester resin material properties (*Fibre Glast, 2018*)

Property[1] of cured casting[3] at 25°C (77°F)	Value (SI)	Value (US)	Method
Barcol Hardness	35	35	ASTM D2583
Tensile Strength	82 MPa	12,000 psi	ASTM D638
Tensile Modulus	3720 MPa	5.4 psi x 10^5	ASTM D638
Tensile Elongation at Yield	4.6%	4.6%	ASTM D638
Tensile Elongation at Break	7.9%	7.9%	ASTM D638
Flexural Strength	131 MPa	19,000 psi	ASTM D790
Flexural Modulus	3450 Mpa	5.0 psi x 10^5	ASTM D790
Heat Distortion Temperature	98°C	209°F	ASTM D648

4.3 Vacuum Infusion Process (VIP)

In the VIP, a vacuum pressure used to suck the resin into a sealed mold by carefully placed tubing. The peel ply is placed between the laminate and vacuum bag for an easy and clean vacuum bag removal. The benefits of VIP are efficient fiber-to-resin ratio, consistency in the resin flow, and cleaner.

VIP Components:

- Vacuum pumps, resin trap and tubing
- Flow media, peel ply and bagging material
- Laminate (Fiberglass, carbon fiber)
- Vinyl ester resins with Styrene thinner (optional)
- A complete line of precision measuring instruments

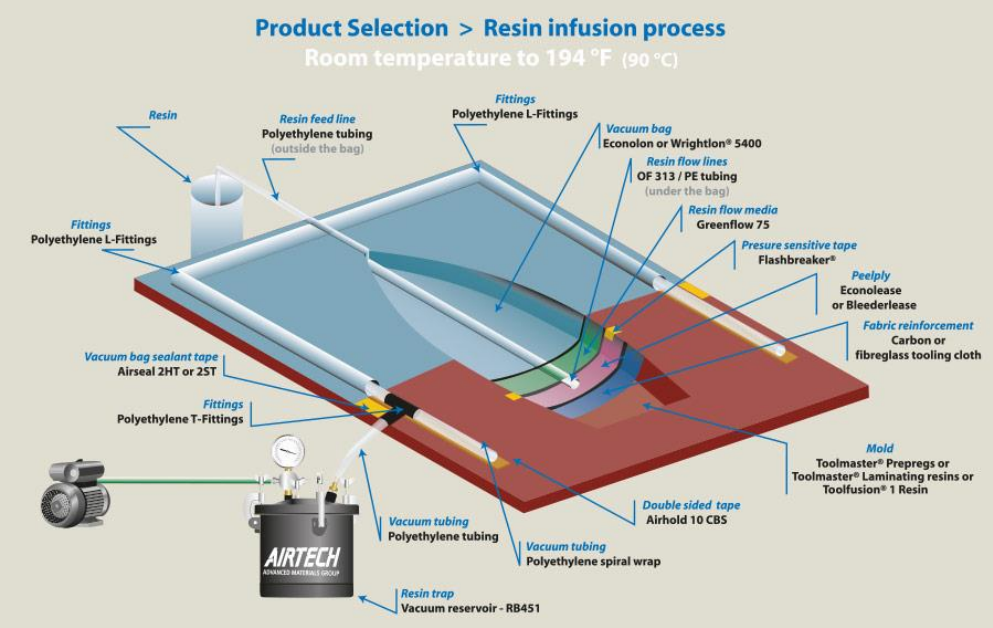

Figure 4-2 Vacuum Infusion Process (VIP) diagram

4.4 Panel Manufacturing

In the current study, unidirectional non-crimp fiber glass was used to make small-scale FRP beams. A fiber glass mat was cut into 12" X 10" sheets. Each panel was made using 31 sheets of glass-fiber, and each sheet is about 0.03 inches (0.79 mm) thick. Vacuum Infusion Process (VIP) was the method utilized to saturate the composite.

Six different FRP samples were made at different times and different atmospheric conditions. In this experiment, the temperature and humidity showed a high impact on the resin

polymerization, flow, and hardening. After running the experiment several times, it was determined that maintaining a perfect vacuum seal was a challenge.

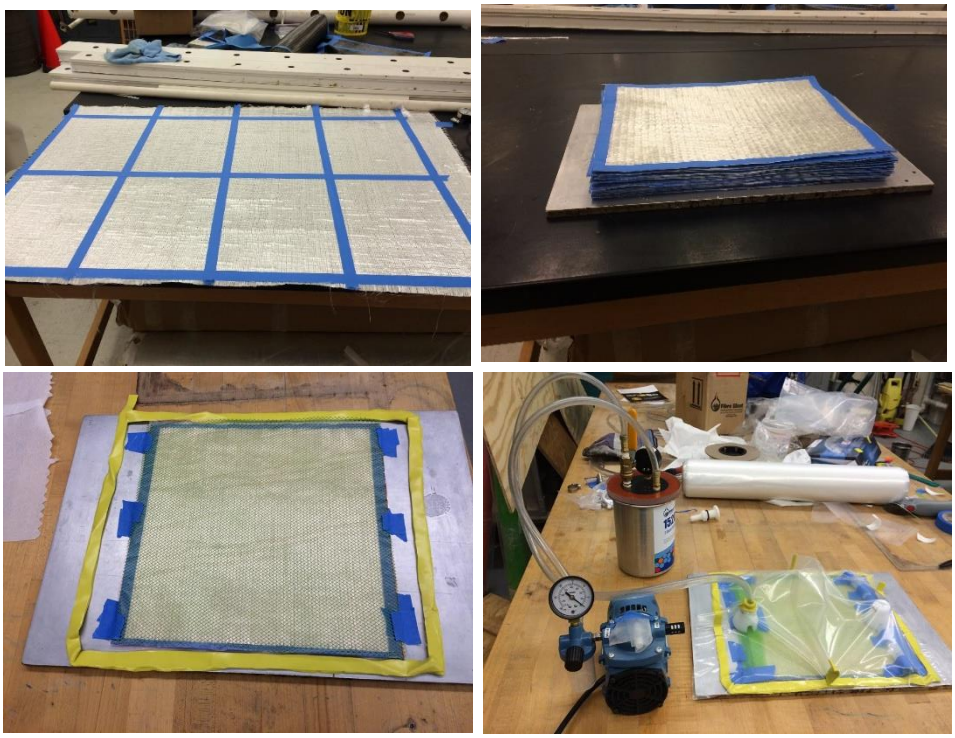

Table 4-3 Climate condition during testing and specimen configuration

	Sample					
	#1	**#2**	**#3**	**#4**	**#5**	**#6**
Number of layers	2	31	31	31	31	31
Layer Orientation	90	90	90	0	0	0
Vacuum Status	Sealed	Leaked	Sealed	Leaked	Sealed	Sealed
Styrene	no	no	no	no	yes	yes
Temperature (f)	72	/	75	75	84	84
In/out door	In	/	out	out	out	out
Weather Status	/	/	Cloudy	Night	Cloudy	Sunny
Humidity (%)	/	/	/	98	70	72
Date	12-Feb	10-Mar	22-Apr	30-May	10-Jun	18-Jun

As shown in the above table, not all samples had a perfect vacuum. It was difficult to detect small leaks in the early stage of the experiment. Vacuum gauges with an ultrasonic leak detector were used to make sure there were no leaks before starting the infusion process.

Only one layer of fiber glass was used in the first sample to simplify the process and become familiar with the VIP. The resin to MEKP ratio was 100:1.25 by weight. In samples #2 and #3, the resin flow was not fast enough to saturate the entire sample before it began to harden. The reason behind the quick setting was that the orientation of the fibers was perpendicular to the resin flow, which makes the friction factor between the fibers and the resin higher. Another reason was the climate condition. It only takes between 25-30 minutes for the resin to cure and

Figure 4-4 FRP sample #5

Figure 4-3 FRP sample #4

harden after mixing it with the MEKP agent. 6% Styrene (resin thinner) was mixed with the resin in sample #5 and #6 for more uniform and faster resin flow. After leaving the specimens at room

temperature for 24 hours to cure and fully harden as was directed by the supplier, they were cut into 1" X 0.7“ X 10“beams for testing. The resin to fiber ratio in sample #5 was 1:1.5 by weight.

4.5 Testing and Results

A Tinius Olsen universal testing machine located in the laboratory at ERAU, was used to test the beams in bending. Four-point bending was applied to only samples #4 and #5. Sample #5 represented the best manufacturing result because it was fully saturated with no leaks in the vacuum bag. Sample #4 contained numerous visible defects and was not completely saturated.

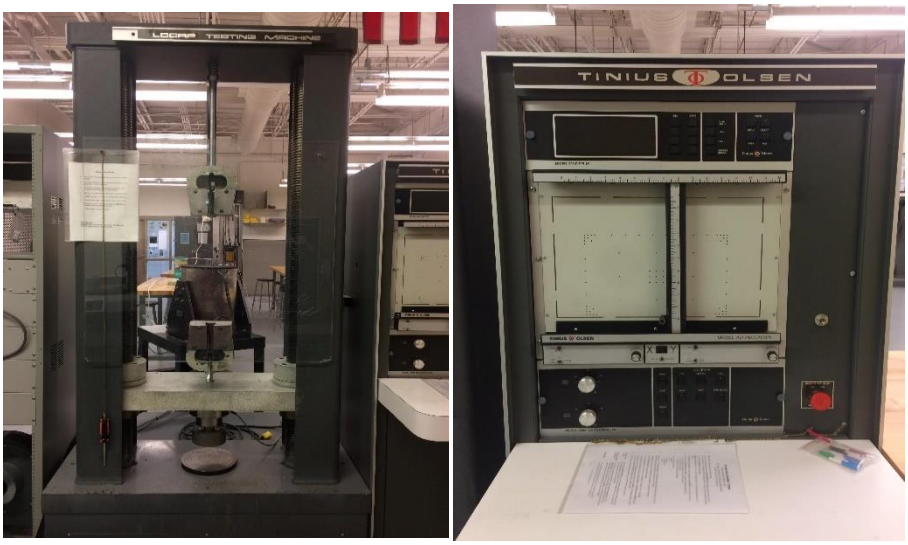

Figure 4-5 Compression machine with plotter

In order to obtain better testing results and avoid localized damage at the load application points, steel bearing pads were glued on the specimens at the load and support locations. Two different span lengths 9-in (228.6 mm) and 4.5-in (114.3 mm) were evaluated. For the 9-in span length, the applied loads were 3 inches (76.2 mm) apart and 3 in away from the support. The applied loads were 1.5 inches apart and 1.5 inches (38.1 mm) away from the support for the 4.5-in specimen.

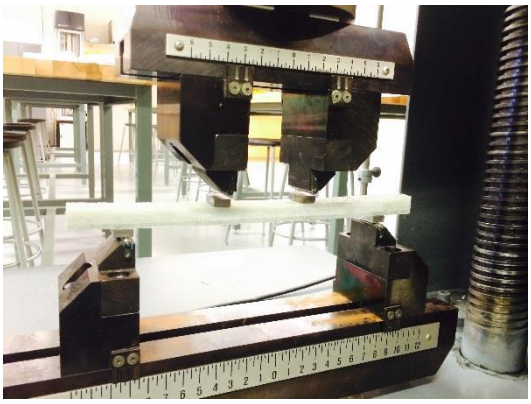

Figure 4-6 9-in span length FRP beam

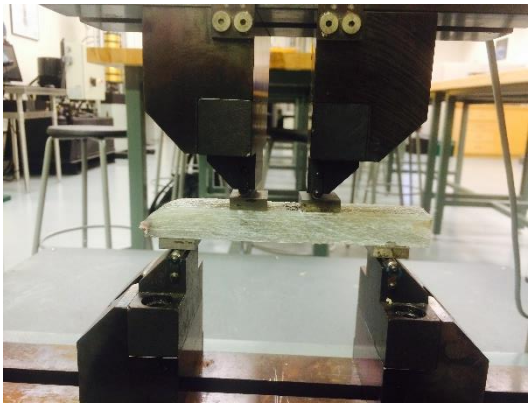

Figure 4-7 4.5-in span length FRP beam

Table 4-4 Results summary

	Samples				
	Long Span		Short Span		
	#5A	#5B	#4	#5C	#5D
Force (lb)	5040	6540	1760	8000	10160
Disp. (in)	0.5	0.4	0.64	0.15	0.2
E (ksi)	6765.37	5377.06	230.71	4474.45	2088.34

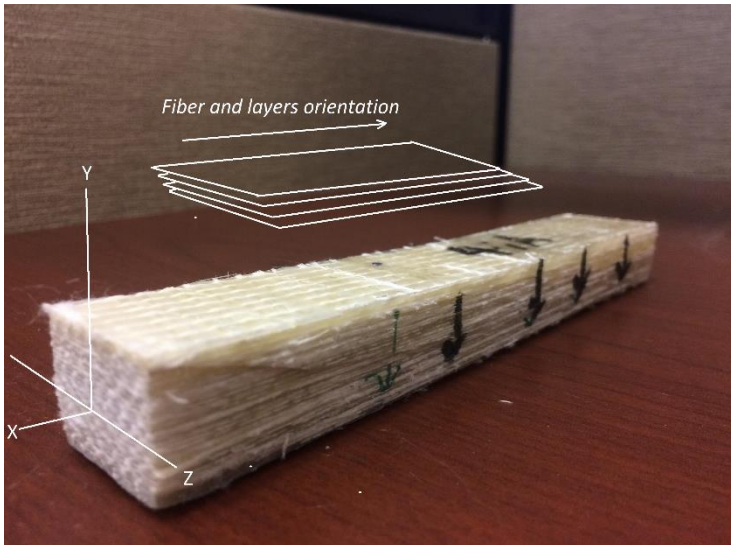

Figure 4-8 GFRP layers and fiber orientation

In sample #4 and #5, the fiber orientation for all layers was in one direction and parallel to the resin flow. During testing, the loads were applied along the Y-axis as shown in figure # for #4, #5A, and #5C specimens. In specimen #5B and #5D, the loads were along the Z-axis. The reason behind using different span length and specimen orientation is to observe the specimens' failure in shear and strength.

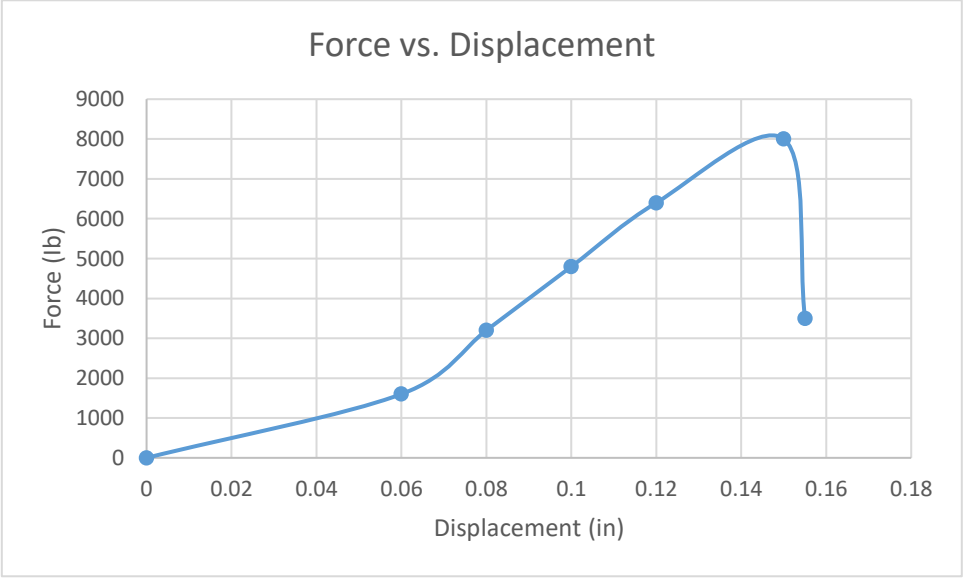

Figure 4-9 Force verses displacement for 4.5 in. #5C specimen

Sample #5C was tested in four-point bending to evaluate the composite stiffness and ultimate strength. The specimen failed at load of 8000 lb load as shown in the pictures above. Shear failure occurred when the deflection reached 0.15-in (3.8 mm). The reason behind having a shear failure rather than compression failure is that the loads applied were along the Y-axis where the FRP layers are stacked on top of each other. It was clear the shear failure happened along the weak axis where the FRP sheets are held together by the resin.

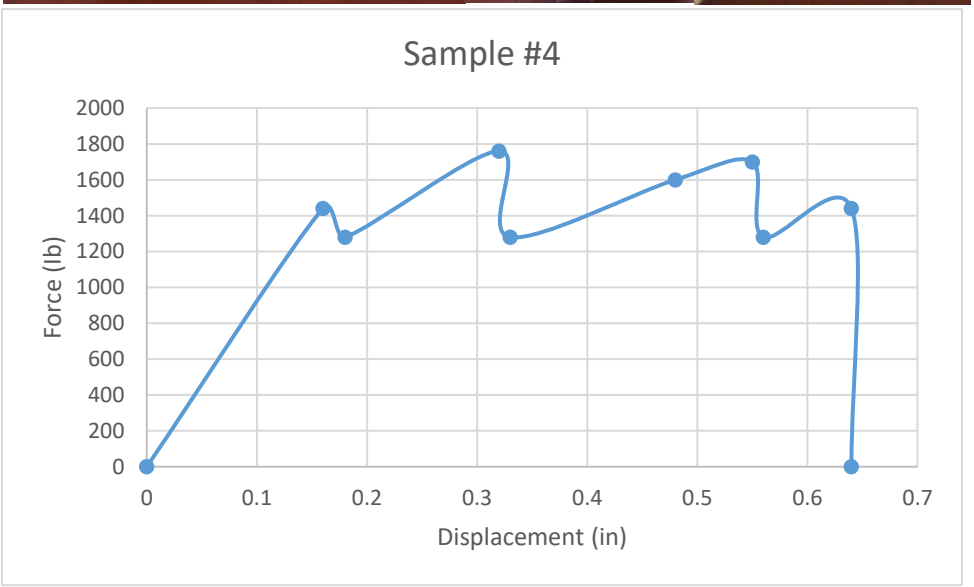

Figure 4-10 Force verses displacement for 4 ½" #4 specimen

Specimen #4 was one of the samples that did not have a perfect vacuum and resin saturation. The result for the 4.5-in (114.3 mm) specimen shows a high deflection with low stiffness. The

sample had 0.64-in (16.3 mm) of deflection under only 1760 lb of force. The failure mode was also a shear failure.

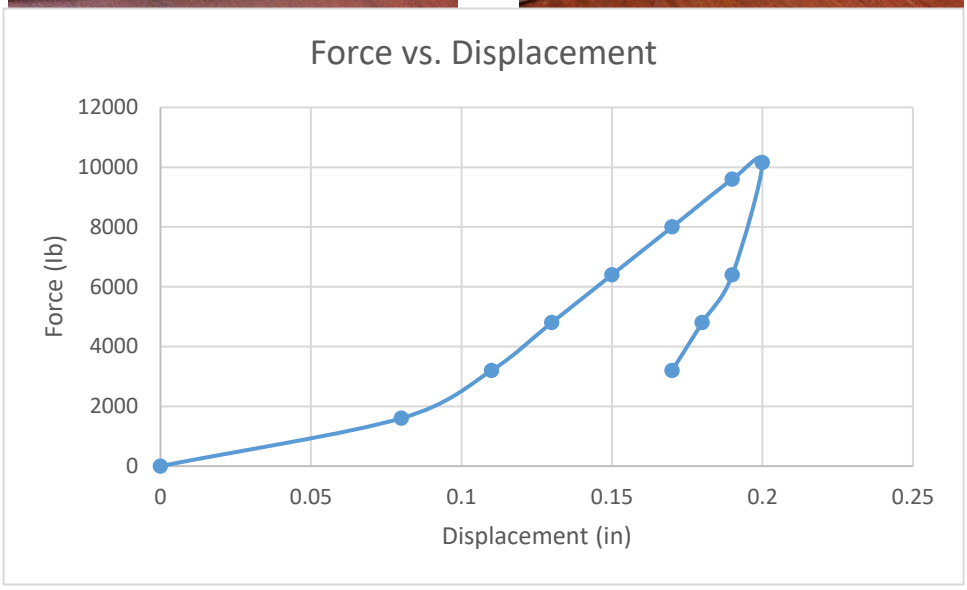

Figure 4-11 Force verses displacement for 4.5 in. #5D specimen

Sample #5D shows a perfect compression failure for a short-span beam. The loads were applied along the Z-axis rather than Y-axis, which resulted in an increase in stiffness. The failure happened after the sample was subjected to 10,160 lb of force, which was the highest of all specimens. Only 0.2 in (5.1 mm) of deflection was experienced by the sample before failure. A 27% increase in sample stiffness was observed when the loads were applied along the strong axis.

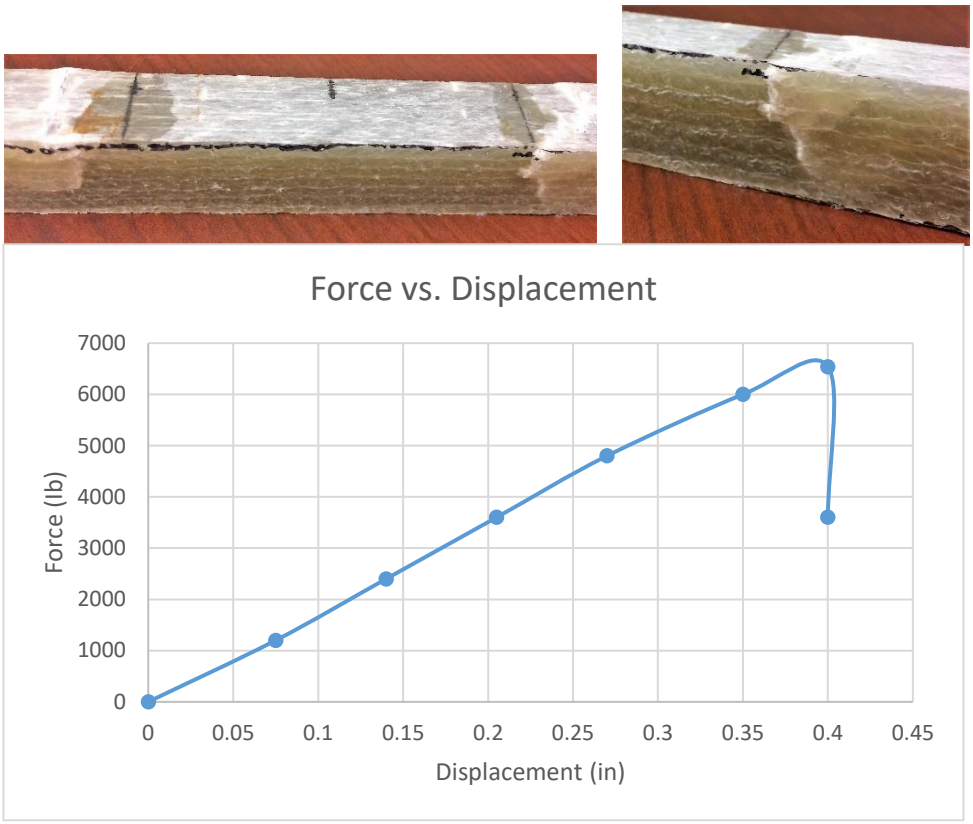

Figure 4-12 Force verses displacement for 9" #5B specimen

Sample #5B was one of the long-span samples that was tested for strength and deflection. The beam was oriented along the strong axis to test for compression failure. A compression failure occurred after applying 6540 lb of force. The sample deflected 0.4-in (10.2 mm) before failure. The cracks happened at the load locations and progressed to the bottom of the sample. As the span-length increased the beam stiffness decreased and the deflection increased.

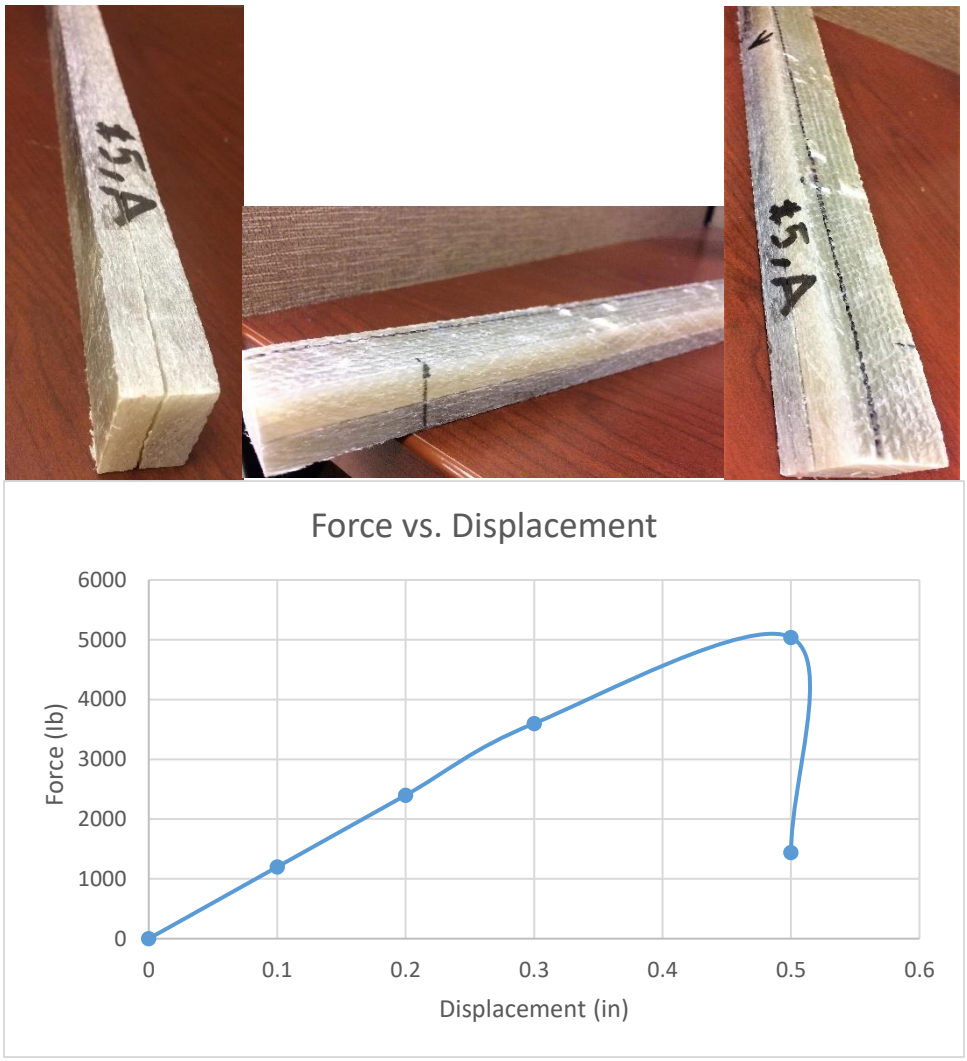

Figure 4-13 Force verses displacement for 9 in. #5A specimen

The last sample tested was sample #5A. This sample was oriented to test for shear failure. The specimen failed at 5040 lb of load with 0.5 in (12.7 mm) of deflection. The beam stiffness dropped about 23% when oriented to test for the weak axis.

The FRP cross-section was constant for all samples. The FRP samples showed high strength when they were oriented to obtain maximum moment of inertia. Sample #5D experienced the

highest applied load before failure; however, the sample modulus of elasticity was low because of the small deflection the sample experienced. The highest modulus of elasticity during testing, that was 6.76 Msi, was observed through sample #5A. The modulus of elasticity of the E-T 1600 is 5.70 Msi. The reason behind the difference in the modulus values is that the fiber density and the amount of resin used in this experiment is not identical to the E-T 1600.

Chapter 5 Conclusion and Recommendations

There are over 600,000 bridges in the United States as was stated by the American of Society of Civil Engineering in 2017. These bridges are designed for a 50-year service life. 67% of these bridges have a span length between 20 ft-to-60 ft. Corrosion is one of the critical issues that these bridges face – especially in salt water environments like in the state of Florida. The material properties for the fiber-reinforced polymer make it a strong candidate for bridge girders in extremely aggressive environments. Three different fiber-reinforced polymer cross-sections, U-girders, concrete-filled FRP tubes, and Double Web Beam, were investigated in this research as a solution for bridge girders in corrosive environments.

The findings from the research completed by the Civil Engineering Department at ERAU combined with the findings of the current study identified the U-girder to be the most efficient and cost effective FRP alternative. Even though the results show that FRP girders are costly compared to other civil engineering materials, they require less maintenance. The service life of the bridge may be possible to extend to 75 years when utilizing FRP into the bridge's superstructure. The simulation results show that only 4 DWB-36 girders are required for a 40 ft span bridge when using a concrete deck. Virginia Route 601 Bridge is a 39 ft long bridge with a lumber deck that was supported by 8 DWB-36 girders. The number of girders was reduced to 50% by incorporating a cast-in-place concrete deck in the bridge design. The VIP method was shown to be an effective technique to manufacture FRP beams; however, maintaining a perfect vacuum bag is challenging even in small-scale beams.

One of the limitations in this study was not having an adequate space and the right equipment to build a bigger scale FRP model. Another limitation was the slow computer processor used to run the simulations. Limited development of established FRP standards for

shear and flexure also made it difficult in decision making when evaluating the strength limit states. This work also required significant assumptions that were based on the current AASHTO LRFD-7 and AASHTO-FRP for concrete-filled tubes.

The method and results of this research can aid in future studies to develop design criteria for all-FRP or hybrid FRP/concrete bridge girders. While this paper has highlighted some of the basics in FRP bridge construction, there are still quite a few outstanding issues that need to be considered. The most important factor that remains unresolved is establishing a shear connection between FRP girders and a cast-in-place RC deck. Inspection and quality assurance for FRP girders is also an area that is ripe for additional research.

References

AASHTO LRFD Guide Specifications for Design of Concrete-Filled FRP Tubes, 1st Edition, 2012.

Abdelgader, H., & Elbaden, A. (2014). Concreting method that produce high modulus of elasticity. MATEC Web of Conferences, 11, 03012. doi:10.1051/matecconf/20141103012. https://www.matec-conferences.org/articles/matecconf/pdf/2014/02/matecconf_cmss2013_03012.pdf

Acquah, C., Datskov, I., Mawardi, A., Zhang, F., Achenie, L. E., Pitchumani, R., & Santos, E. (2006). Optimization under uncertainty of a composite fabrication process using a deterministic one-stage approach. *Computers & Chemical Engineering*,*30*(6-7), 947-960. doi:10.1016/j.compchemeng.2005.12.015.

American Association of State Highway and Transportation Officials (AASHTO). (2014). AASHTO LRFD Bridge Design Specifications, 7th Edition. Washington, D.C.: AASHTO.

ASCE. (2017). Bridges. Retrieved from infrastructure report card: http://www.infrastructurereportcard.org/cat-item/bridges/

Berke, N. S., Chaker, V., & Whiting, D. (1990). *Corrosion rates of steel in concrete*. Philadelphia, PA: American Society for Testing and Materials.

Brown, J. R., Tamijani, A., & Papapetrou, V. (2018). Bridge Girder Alternatives for Extremely Aggressive Environments (Rep. No. Unknown). Tallahassee, Florida: Florida Department of Transportation.

Cai, Z., & Ross, R. (unknown). Mechanical Properties of Wood-Based Composite Materials. Retrieved from https://www.fpl.fs.fed.us/documnts/fplgtr/fplgtr190/chapter_12.pdf.

Chen et al. (2009). Experimental Characterization and Optimization of Hybrid FRP/RC Bridge Superstructure System. Journal of Bridge Engineering, Vol. 14, No. 1, January 1, 2009. http://ascelibrary.org/doi/pdf/10.1061/%28ASCE%291084-0702%282009%2914:1%2845%29

Cousins, T. E., & Lesko, J. J. (2005). *Construction of a Virginia Short-Span Bridge with the Strongwell 36-Inch Double-Web I-Beam* (Tech. No. FHWA/VTRC 06-CR5). Charlottesville, Virginia: Virginia Department of Transportation and the University of Virginia.

Cousins et al. (2005). Construction of a Virginia Short-span Bridge with the Strongwell 36-inch Double-web I-Beam. VCTIR No. 06-CR5. http://vtrc.virginiadot.org/PubDetails.aspx?PubNo=06-CR5

Cousins, T. E., & Neely, W. D. (2003). *EVALUATION OF THE IN-SERVICE PERFORMANCE OF THE TOM'S CREEK BRIDGE FIBER-REINFORCED*

POLYMER SUPERSTRUCTURE (Tech. No. VTRC 04-CR5). Charlottesville, Virginia: Virginia Department of Transportation and the University of Virginia.

CYTEC. (2014). *Composite Materials for Marine Applications*.

Durham, S. A., Heymsfield, E., & Tencleve, K. D. (2007). Cracking and Reinforcement Corrosion in Short-Span Precast Concrete Bridges. *Journal of Performance of Constructed Facilities,21*(5), 390-397. doi:10.1061/(asce)0887-3828(2007)21:5(390)

Hurd, M. K. (1985). ECONOMICAL SHORT SPAN CONCRETE BRIDGES. Retrieved from Concrete Construction https://www.concreteconstruction.net/how-to/construction/economical-short-span-concrete-bridges_o.

Image obtained from Fibreglast website (http://www.fibreglast.com/product/Continuous_Strand_Mat_251/ Fiberglass_Mat). Accessed August 11, 2017

Johnson, A. B. (2007). American Iron and Steel Institute. *Steel Bridge Construction: Myths & Realities,7*, d432. Retrieved from NCDOT https://connect.ncdot.gov/resources/Structures/Structures Seminars/10 - Myths and Realities of Steel Bridges.pdf.

MFG Corporation (Unknown Date). FRP BRIDGE EVOLUTION: TxDOT ADVANCES VIABILITY OF CUSTOM FRP BRIDGE BEAMS IN NEW HYBRID STRUCTURAL CONSTRUCTION RESEARCH PROJECT. http://www.mfgcp.com/_files/docs/file_13.pdf

Nayak, N. V. (2014). Internatinal Journal of Scientific and Research Publication. Composite Materials in Aerospace Applications,4(9). Retrieved from https://scholar.google.com/scholar?q=Composite Materials in Aerospace Applications Nikhil V Nayak&hl=en&as_sdt=0&as_vis=1&oi=scholart.

Papapetrou, V. S., Tamijani, A. Y., Brown, J., & Kim, D. (2018). Design Optimization of Hybrid FRP/RC Bridge. Applied Composite Materials. doi:10.1007/s10443-018-9691-3. https://link.springer.com/article/10.1007/s10443-018-9691-3

Prestressed Florida-I Beams, Index 20010 Series (2016). Retrieved from http://www.fdot.gov/roadway/DS/17/IDS/IDS-20010.pdf

Reitmann, B. (2007). San Patricio Fiber Reinforced Polymer (FRP) Bridge. Bill Reitmann, P.E. Texas Department of Transportation. Retrieved from FTP. dot https://ftp.dot.state.tx.us/pub/txdot-info/des/presentations/desbrgconf07/reitmann frp_bridge.pdf.

Restrepo, E. S. (2002). Determination of AASHTO bridge design parameters through field evaluation of the Rt. 601 bridge: A bridge utilizing Strongwell 36 in. fiber-reinforced polymer double web beams as the main load carrying members (Unpublished master's thesis).

Schniepp, T. J. (2002). Design manual development for a hybrid, FRP double-web beam and characterization of shear stiffness in FRP composite beams (Unpublished master's thesis).

Strongwell Corporation (2003). EXTREN DWB Design Guide. http://www.strongwell.com/wp-content/uploads/2013/03/EXTREN-DWB-Design-Guide.pdf

U.S. Department of Transportation. (2015). Steel Bridge Design Handbook. *Corrosion Protection of Steel Bridge,19*. Retrieved from FHWA https://www.fhwa.dot.gov/bridge/steel/pubs/hif16002/volume19.pdf

User, S. (unknown). Performancecomposites. Retrieved from http://www.performancecomposites.com/

User, S. (unknown). Performancecomposites. Retrieved from http://www.performancecomposites.com/images/Fiberglass-and-Composite-Material-Design-Guide.pdf

Vectorply, (2015), retrieved from http://vectorply.com/wp-content/uploads/2015/06/E-T-1600.pdf

Vinyl Ester Resin. (2018). Retrieved from https://www.fibreglast.com/product/General_Purpose_Vinyl_Ester_Resin_just_resin_1110/fiberglass-repair.

Wallenberger,, F. T., Watson,, J. C., & Li, H. (2001). Glass Fibers, 21. Retrieved from https://www.asminternational.org/documents/10192/1849770/06781G_p27-34.pdf.

Williams, J. (2008). The Ongoing Evolution of FRP Bridges. Public Roads (FHWA-HRT-08-006), Vol. 72, No. 2, Sept/Oct 2008. https://www.fhwa.dot.gov/publications/publicroads/08sep/03.cfm

Yousefpour, A., & Nejhad, M. N. (2004). Design, Analysis, Manufacture, and Test of APC-2/AS4 Thermoplastic Composite Pressure Vessels for Deep Water Marine Applications. *Journal of Composite Materials,38*(19), 1701-1732. doi:10.1177/0021998304044765

Zhao, L. et al. (2000). Preliminary Evaluation of the Hybrid Tube Bridge System. California Department of Transportation Report No. TR-2000/04. http://www.dot.ca.gov/hq/esc/earthquake_engineering/Research/modgirde.pdf

Zoghi, M. (2014). *The international handbook of FRP composites in civil engineering*. Boca Raton, FL: CRC Press/Taylor & Francis Group.

Appendix A: Monte-Carlo Simulation

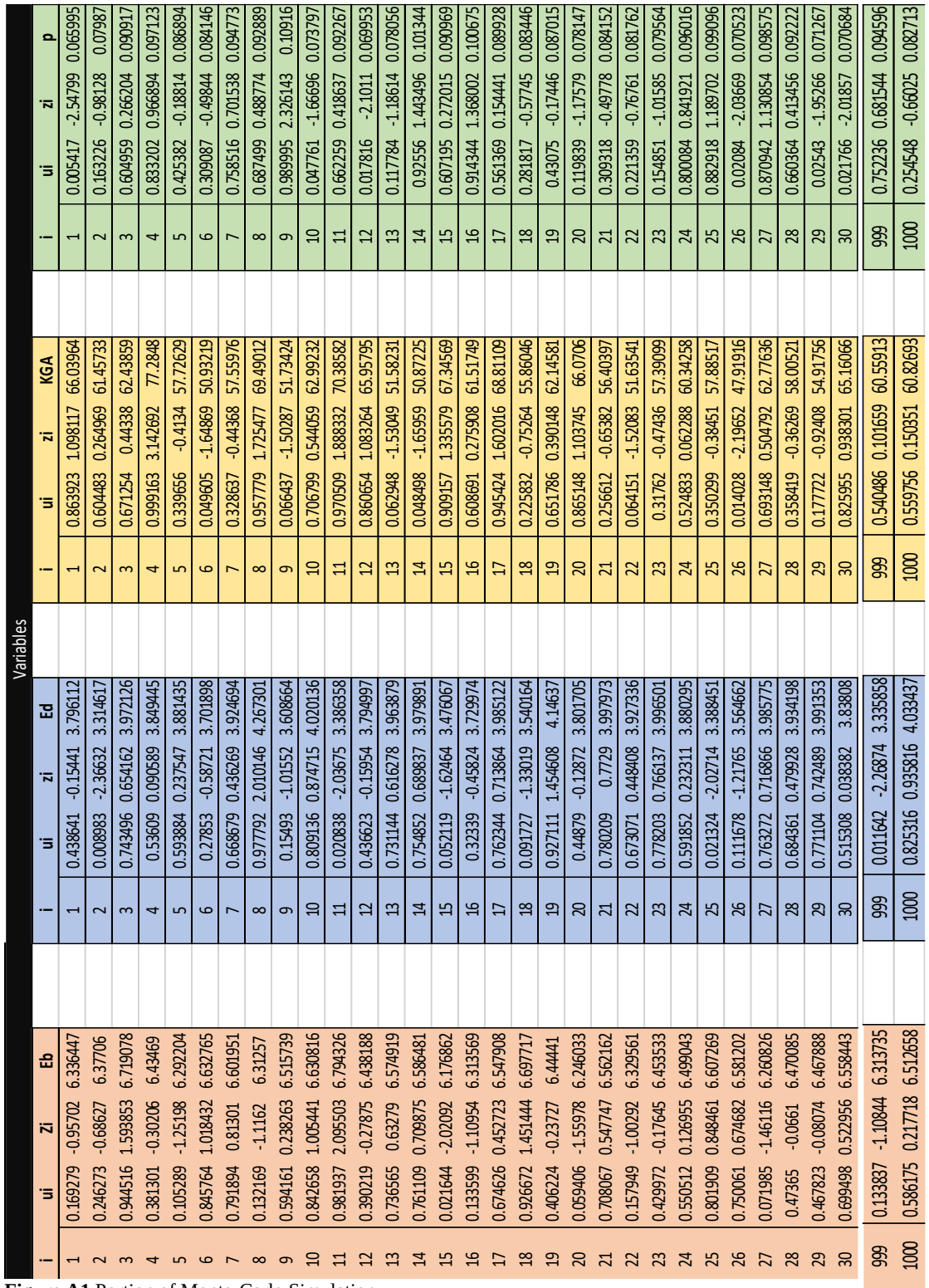

| Variables | | |

Appendix B: Distribution Mode for FRP, Concrete, and Timber

i	E (Msi)	i/N
1	6.02	0.05
2	6.21	0.1
3	6.27	0.15
4	6.28	0.2
5	6.37	0.25
6	6.38	0.3
7	6.39	0.35
8	6.4	0.4
9	6.44	0.45
10	6.49	0.5
11	6.52	0.55
12	6.52	0.6
13	6.61	0.65
14	6.63	0.7
15	6.64	0.75
16	6.66	0.8
17	6.67	0.85
18	6.7	0.9
19	7.27	0.95
Mean	**6.46**	
Std.dev	**0.18**	

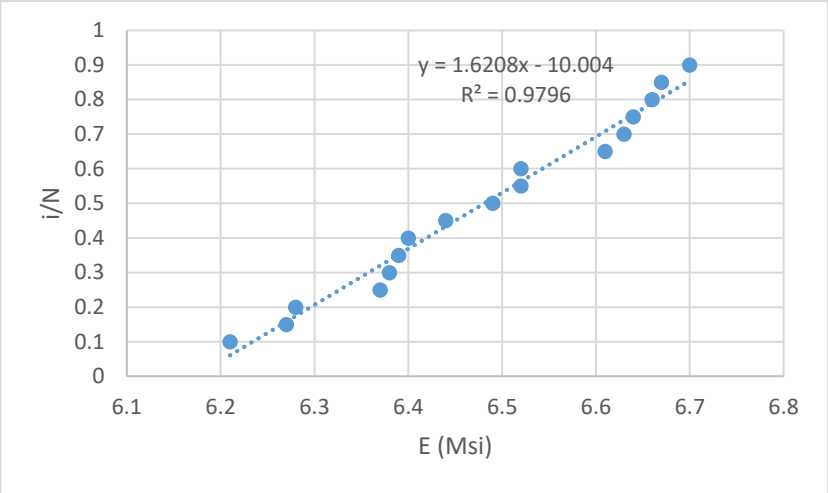

Figure B1 Normal distribution for the modulus of elasticity of the FRP material

i	kGA (Msi-in^2)	i/N
1	33.6	0.05
2	33.9	0.1
3	38	0.15
4	39.5	0.2
5	42.1	0.25
6	43.4	0.3
7	43.9	0.35
8	44.5	0.4
9	46.2	0.45
10	47.2	0.5
11	47.3	0.55
12	49.1	0.6
13	50.3	0.65
14	51.6	0.7
15	52.3	0.75
16	53.5	0.8
17	58.5	0.85
18	62.4	0.9
19	66.9	0.95
Mean	**47.59**	
Std.dev	**8.84**	

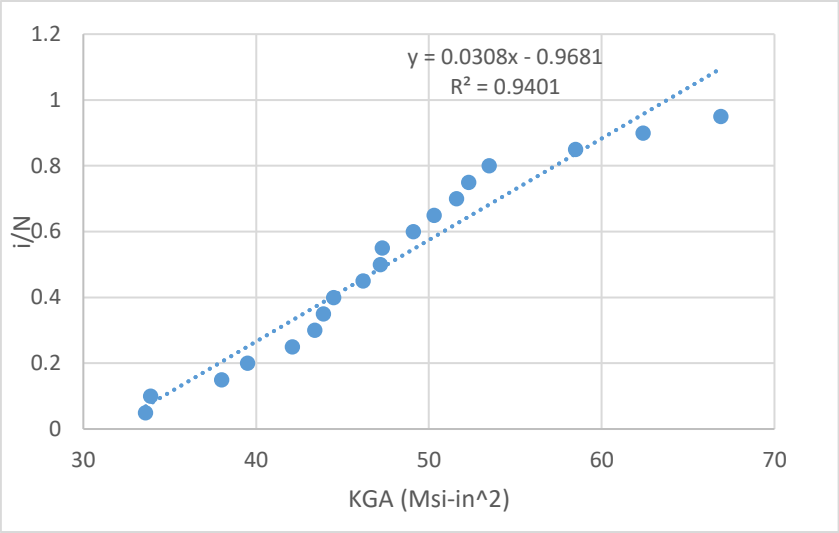

Figure B2 Normal distribution of the shear stiffness of the FRP material

i	Gpa	i/N
1	9.07	0.05
2	9.3	0.09
3	9.44	0.14
4	10.3	0.18
5	10.8	0.23
6	11.2	0.27
7	12.2	0.32
8	12.2	0.36
9	12.3	0.41
10	12.3	0.45
11	12.3	0.50
12	12.8	0.55
13	12.8	0.59
14	12.9	0.64
15	13	0.68
16	13	0.73
17	13.4	0.77
18	13.5	0.82
19	13.6	0.86
20	13.9	0.91
21	14.1	0.95
Mean	**12.11**	
St.dev.	**1.52**	

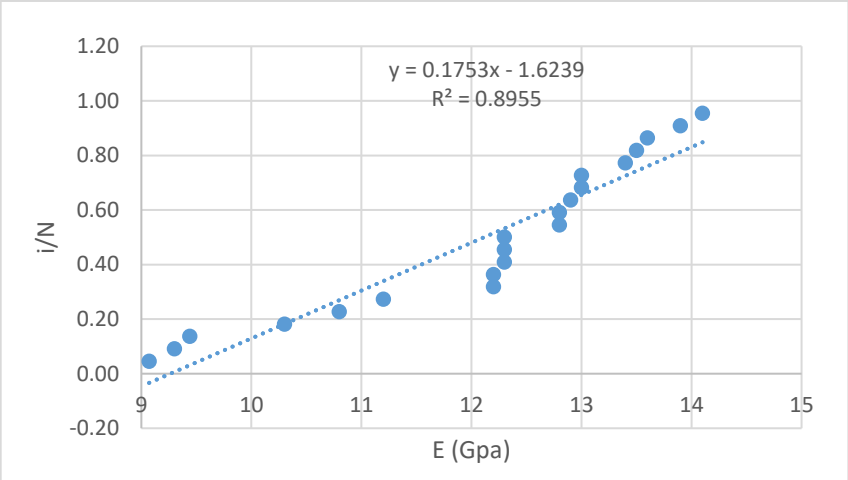

Figure B3 Normal distribution of the modulus of elasticity of wood

i	E(Msi)	i/N
1	3.56	0.1
2	3.57	0.2
3	3.58	0.3
4	3.82	0.4
5	3.83	0.5
6	3.87	0.6
7	4.07	0.7
8	4.08	0.8
9	4.08	0.9
Mean	**3.83**	
Std.dev.	**0.22**	

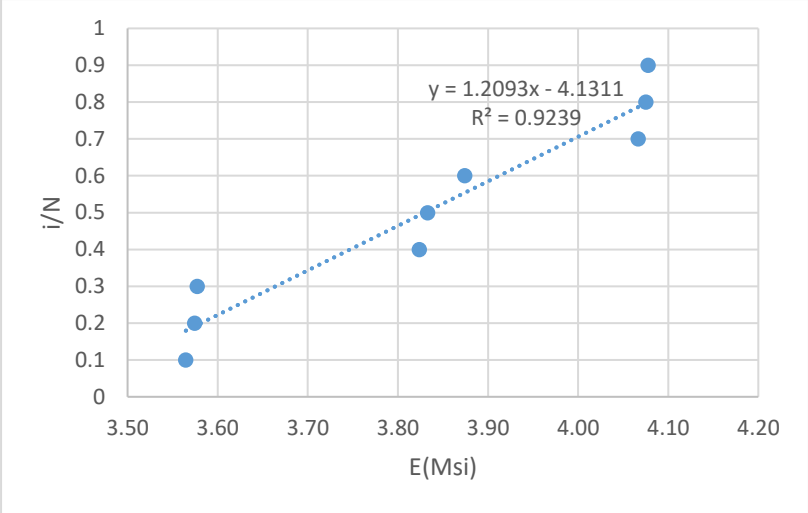

Figure B4 Normal distribution of the modulus of elasticity of concrete